UNCLASSIFIED

SECURITY CLASSIFICATION OF THIS PAGE *(When Data Entered)*

REPORT DOCUMENTATION PAGE

READ INSTRUCTIONS BEFORE COMPLETING FORM

1. REPORT NUMBER: AFIT/CI/NR 88- 110
2. GOVT ACCESSION NO.:
3. RECIPIENT'S CATALOG NUMBER:
4. TITLE *(and Subtitle)*: A BROAD-BAND ARRAY OF APERTURE-COUPLED CAVITY-BACKED SLOT ELEMENTS
5. TYPE OF REPORT & PERIOD COVERED: MS THESIS
6. PERFORMING ORG. REPORT NUMBER:
7. AUTHOR(s): JOSEPH MICHAEL BURNS
8. CONTRACT OR GRANT NUMBER(s):
9. PERFORMING ORGANIZATION NAME AND ADDRESS: AFIT STUDENT AT: UNIVERSITY OF ILLINOIS URBANA - CHAMPAIGN
10. PROGRAM ELEMENT, PROJECT, TASK AREA & WORK UNIT NUMBERS:
11. CONTROLLING OFFICE NAME AND ADDRESS:
12. REPORT DATE: 1988
13. NUMBER OF PAGES: 82
14. MONITORING AGENCY NAME & ADDRESS *(if different from Controlling Office)*: AFIT/NR Wright-Patterson AFB OH 45433-6583
15. SECURITY CLASS. *(of this report)*: UNCLASSIFIED
15a. DECLASSIFICATION/DOWNGRADING SCHEDULE:

AD-A196 400

16. DISTRIBUTION STATEMENT *(of this Report)*: DISTRIBUTED UNLIMITED: APPROVED FOR PUBLIC RELEASE

DTIC ELECTE AUG 0 4 1988 H

17. DISTRIBUTION STATEMENT *(of the abstract entered in Block 20, if different from Report)*: SAME AS REPORT

18. SUPPLEMENTARY NOTES: Approved for Public Release: IAW AFR 190-1
LYNN E. WOLAVER
Dean for Research and Professional Development
Air Force Institute of Technology
Wright-Patterson AFB OH 45433-6583

19. KEY WORDS *(Continue on reverse side if necessary and identify by block number)*:

20. ABSTRACT *(Continue on reverse side if necessary and identify by block number)*: ATTACHED

DD FORM 1 JAN 73 1473 EDITION OF 1 NOV 65 IS OBSOLETE

UNCLASSIFIED

SECURITY CLASSIFICATION OF THIS PAGE *(When Data Entered)*

ABSTRACT

A Broad-Band Array of Aperture-Coupled Cavity-Backed Slot Elements

A broad-band array of aperture-coupled cavity-backed slot (CBS) elements was designed, constructed and tested. The antenna array design incorporated two major departures from previous CBS arrays: aperture coupling, and 'half-width' cavities. Expiremental results demonstrated these departures enhance the potential for larger operating bandwidths using less physical space than previous arrays of CBS elements. Computer simulation and test results also indicated that the antenna array was not hindered by the presence of a large structural stopband such as was observed in all previous CBS arrays. Consequently, modulation of the antenna feedline impedance was not required for satisfactory performance. Antenna patterns for the array were similar over the frequency range 1.75 - 3.5 GHz.

A BROAD-BAND ARRAY OF APERTURE-COUPLED CAVITY-BACKED SLOT ELEMENTS

BY

JOSEPH MICHAEL BURNS

B.E.E., AUBURN UNIVERSITY, 1981

THESIS

Submitted in partial fulfillment of the requirements
for the degree of Master of Science in Electrical Engineering
in the Graduate College of the
University of Illinois at Urbana-Champaign, 1987

Urbana, Illinois

ACKNOWLEDGEMENTS

There are many besides the author who made this paper possible. The author wishes to thank his advisor, Professor Paul E. Mayes, for his superb guidance, patience, and prodding. He would also like to express his appreciation to Jeff Kromer for expertly building the antennas discussed herein; Jim Drewniak for his training in antenna design, construction and testing; Hugh Smith, Tom Sons, and Dave Tammen for sacrificing countless hours in an effort to obtain antenna patterns for this report; and all the other people in the Electromagnetics and Electromagnetic Communication Laboratories who helped with this research over the last year.

In addition, the author would like to thank his office mates, Captain Charles F. Smith and Captain Mark A. Mehalic, for their assistance with the computer programs in the appendices of this report. Others whose help contributed to this research include the Air Force Institute of Technology, who paid the author's tuition and fees; TRW, Incorporated, who provided funding (a portion of which went directly to this work) for research on slot antennas; and Professor Weng C. Chew, whose enthusiastic, enlightening and patient teaching of an early electromagnetics course sparked the author's interest in this subject.

Of course, the author wishes to express loving thanks to his wife Cindy, and their children Melissa, Amanda, Daniel, and Timothy for their support, understanding, prayers, and love. Finally, and most importantly, the author wishes to thank Almighty God for demonstrating many times during this work that 'I can do all things through Christ who gives me strength.'

TABLE OF CONTENTS

LIST OF TABLES

LIST OF FIGURES

Figure Page

CHAPTER 1
INTRODUCTION

In recent years, there has been a burgeoning interest in low-profile, wide-band antennas. Low-profile antennas have numerous applications, especially for missiles and aircraft, because only these antennas can be conformally mounted. The most popular types of thin antennas are the microstrip patch and the cavity-backed slot (CBS). Much research has been done on both types, but the project reported herein involves only CBS antennas. The main objective of this research is to extend the operating bandwidth of a log-periodic (LP) array of thin CBS elements.

Research on CBS antennas dates back more than thirty years. Mayes provides a good summary of early research and recent progress in developing low-profile, wide-band CBS antennas in his report Very Wide Band Antennas for Missile Fuze Applications [1]. One problem encountered in early attempts to design log-periodic arrays of CBS elements was the structural stopband which occurs in a periodic array of such elements. In this band of frequencies there is no propagation down the feedline. When a corresponding region of attenuation occurs between the feedpoint and the active region of a log-periodic cavity-backed slot (LPCBS) array, the wave launched at the input is mostly reflected before it reaches the active (radiating) region. The structural stopband is caused by additive reflections from discontinuities presented by the slots. Ingerson and Mayes [2] found that modulating the feedline impedance was an effective way of eliminating the stopband. Building on their work, Ostertag [3] designed an LPCBS array using smaller cavity depths and obtained a 50 Ω mean impedance through use of a computer-synthesized modulated impedance feedline. More

recently Tammen's research [4] focused on eliminating the structural stop-bands associated with many LP antennas by combining CBS and monopole elements. Finally, Szmurlo [5] concentrated on increasing the bandwidth of an LPCBS array while using very thin cavities of constant depth and optimizing the design of the modulated impedance feedline. The bandwidth achievable by antennas of his design is limited because of the immense amount of space they require.

The goals of this research were to design and build an LPCBS antenna which has a larger operating bandwidth, uses less 'real estate', and operates at much higher frequencies with a larger power gain than previous LPCBS arrays. Achieving these goals requires taking several large steps forward from the work done by Szmurlo. First, in an effort to reduce losses, the antenna was designed to have air-filled cavities rather than Rexolite-filled ones. Second, the cavities were to be excited by aperture coupling, that is, energy would be coupled into the cavity through an aperture in the bottom of the cavity rather than through the radiating slot in the top of the cavity. Third, a new theory would be applied that allowed each elemental cavity to be built only half as wide as Szmurlo's elemental cavities. This theory and application will be discussed in more detail in Chapter 2. Finally, it was desired that this new antenna would operate at higher frequencies than any previous LPCBS. The high frequency testing of the new antenna led to previously unseen problems, as will be pointed out in Chapter 4.

CHAPTER 2
ANTENNA DESIGN AND CONSTRUCTION

Before constructing an LP array of CBS antennas that introduced several new departures from the previous case, it was considered prudent to test several prototype elements. From the testing of these prototypes, the scaling factor (τ) and many other useful design criteria used in the LP array were determined.

This chapter will focus on the design and construction of these prototypes. The testing of these prototypes and the selection of design criteria will be discussed in detail in Chapters 3 and 4.

2.1 Szmurlo's Antenna

Since this research was, in many ways, a continuation of Szmurlo's, it is useful to have a more detailed understanding of his antenna. A description from his thesis follows.

> The antenna was constructed from a 1/8-inch sheet of Rexolite 2200. An aluminum sheet (also 1/8 inch) was used as backing for the Rexolite to provide support and to provide threaded holes for the screws. The brass screws that form the vertical cavity walls were approximately 1/2 inch apart for the four largest cavities and about 3/8 inch apart for the remainder. These spacings had been determined adequate to make the S-parameters of an isolated cavity-backed slot with screw walls agree very well with those of one with solid walls. Copper cladding forms the top and bottom walls. A slot was cut into the top cavity wall by removing the copper cladding to allow the cavity to radiate when excited. A drawing of the cavities formed on the Rexolite is shown in Figure 1.
>
> To excite the cavities, a microstrip feed is passed over the slot of each cavity. It was found that for symmetrical patterns, the slot should be fed from the center. The feedline was constructed on a 1/16-inch sheet of Rexolite 2200. The characteristic impedance of the feedline was trimmed to 50 ohm

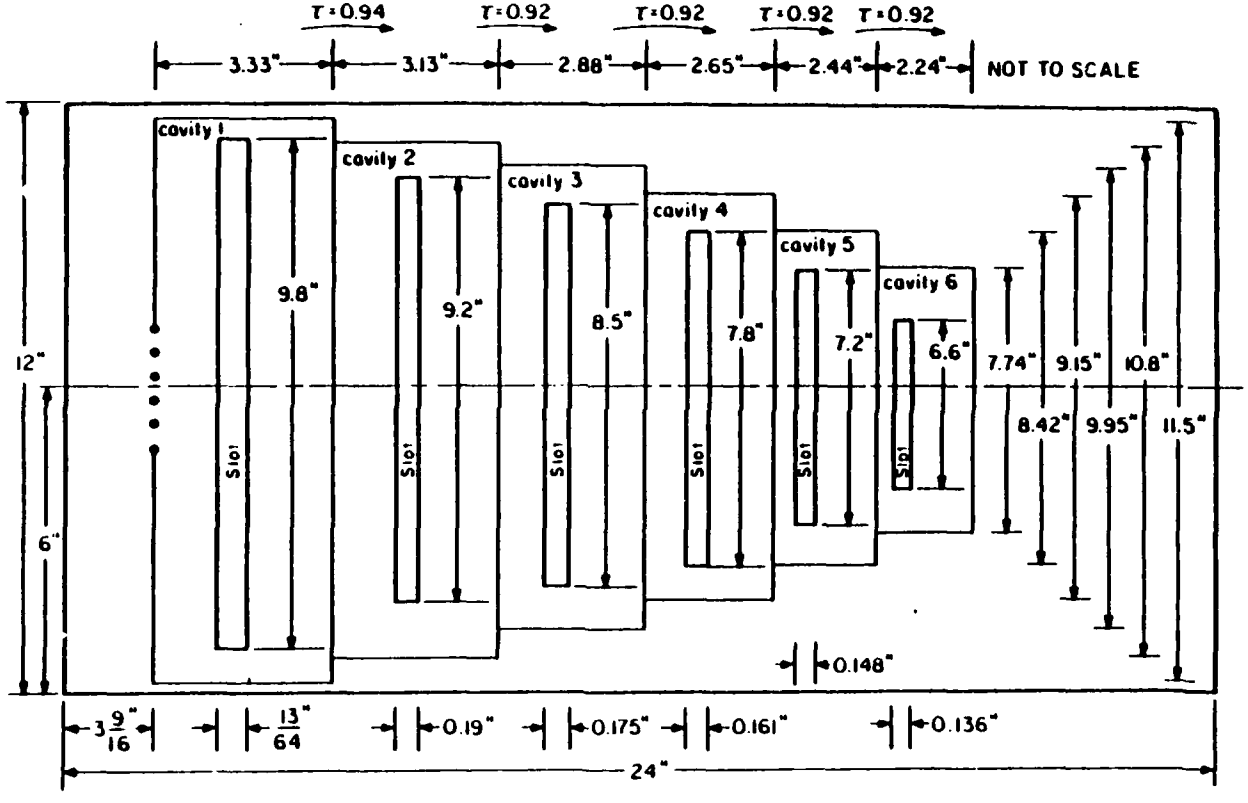

Figure 1. Szmurlo's antenna [5].

by observing its response when tested with a TDR. After using the TDR, the copper ground plane of the feed was cut away where it would lay over the cavity slot. Good contact between the ground plane and the cavity top wall must be maintained, particularly in the vicinity of the slot, or antenna performance will degrade.

A type N female bulkhead connector is present at both ends of the feed. This allows for the measurement of reflection and transmission coefficients of the antenna [5].

The antenna built by Szmurlo operated from 975 to 1325 MHz.

2.2 Cavity Design

As mentioned previously, the antenna was designed utilizing a theory that allowed each elemental cavity to be built half as wide as elemental cavities in previous CBS antennas. This theory was first proposed by Tanner [6]. The basis for the bisection of the cavity can be seen by first analyzing a closed cavity which is very thin (as compared to a wavelength) in the z direction as shown in Figure 2.

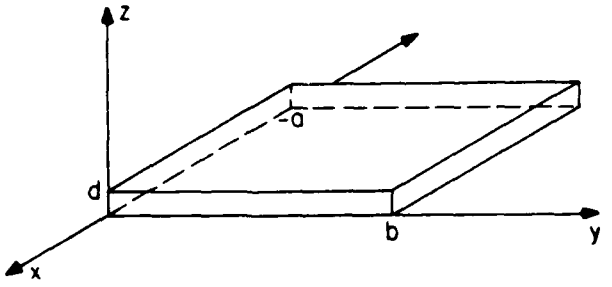

Figure 2. Closed cavity, $d \ll \lambda$.

For the transverse magnetic (TM) case, the time-harmonic ($e^{j\omega t}$ time dependence suppressed) fields inside this cavity can be written as:

$$E_z = E_{mnp} \sin \frac{m\pi x}{a} \sin \frac{n\pi y}{b} \qquad [7] \qquad (2.1)$$

$$H_x = \frac{-j\omega\epsilon\, E_{mnp}}{\left(\frac{m\pi}{a}\right)^2 + \left(\frac{n\pi}{b}\right)^2} \frac{n\pi}{b} \sin\left(\frac{m\pi x}{a}\right) \cos\left(\frac{n\pi y}{b}\right) \qquad [7] \qquad (2.2)$$

$$H_y = \frac{j\omega\epsilon\, E_{mnp}}{\left(\frac{m\pi}{a}\right)^2 + \left(\frac{n\pi}{b}\right)^2} \frac{m\pi}{a} \cos\left(\frac{m\pi x}{a}\right) \sin\left(\frac{n\pi y}{b}\right) \qquad [7] \qquad (2.3)$$

where the z dependence has been dropped because of the thinness in the z direction. Substituting the equation for E_z into the Helmholtz equation, $(\nabla^2 + \beta^2) E_z = 0$, yields the dispersion relation

$$\omega^2 \mu_o \epsilon_o = \left(\frac{m\pi x}{a}\right)^2 + \left(\frac{n\pi y}{b}\right)^2 \qquad (2.4)$$

Solving this equation for ω yields

$$\omega_{mn} = \frac{1}{\sqrt{\mu_o \epsilon_o}} \left[\left(\frac{m\pi}{a}\right)^2 + \left(\frac{n\pi}{b}\right)^2\right]^{1/2} \qquad (2.4a)$$

which is the resonant frequency of the mn mode of this cavity. One can also note from the field equation E_z (with $m = n = 1$) that as x is held constant and y is varied, E_z reaches a maximum at $y = b/2$. Furthermore, at $y = b/2$, $H_x = 0$ for the TM_{110} mode. Thus, an H wall (a surface along which $H_{TAN} = 0$) can be inserted in the plane (x, b/2, z) without interfering with the fields of the cavity. (Note: in most previous rectangular CBS antennas, the radiating slot was placed along the line (x, b/2, d)). A top view of this cavity with the H wall inserted would look like Figure 3.

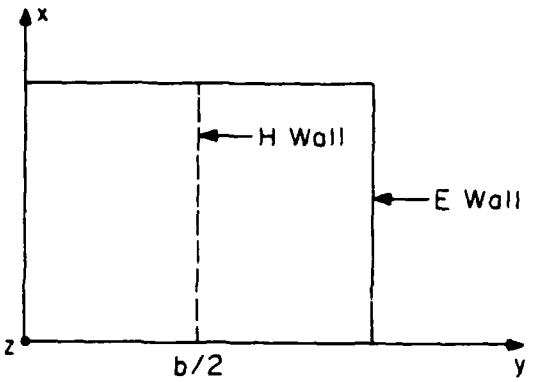

Figure 3. Top view of cavity with H wall.

Next, consider a cavity that has a top view much like half of the cavity in Figure 3. Pictorially, a top view of this cavity would look like Figure 4 below.

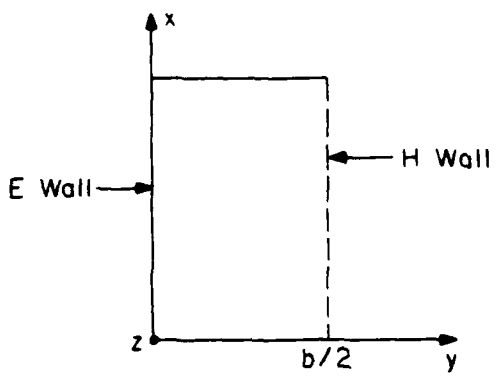

Figure 4. Top view of modified cavity.

One three-dimensional realization of this cavity is shown in Figure 5.

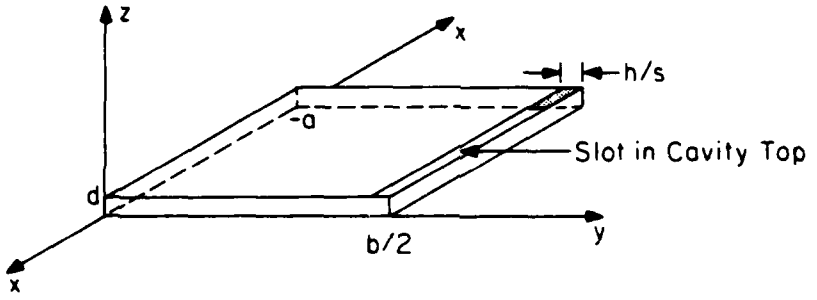

Figure 5. Modified cavity with slot.

To determine the field equations of this modified cavity, begin with the phasor form of Maxwell's equation

$$- \nabla \times \hat{z}\, E_z = j\, \omega \mu_o \vec{H} \tag{2.5}$$

or, using rectangular coordinates and writing the curl as a determinant yields

$$- \begin{vmatrix} \hat{x} & \hat{y} & \hat{z} \\ \frac{\partial}{\partial x} & \frac{\partial}{\partial y} & \frac{\partial}{\partial z} \\ 0 & 0 & E_z \end{vmatrix} = j\omega\mu_o \vec{H} \tag{2.6}$$

$$= - \left(\hat{x}\, \frac{\partial E_z}{\partial y} - \hat{y}\, \frac{\partial E_z}{\partial x}\right) = j\omega\mu_o \vec{H} \tag{2.7}$$

$$\text{Therefore } \vec{H} = \frac{1}{j\omega\mu_o} \left(\hat{y}\, \frac{\partial E_z}{\partial x} - \hat{x}\, \frac{\partial E_z}{\partial y}\right) \tag{2.8}$$

To find E_z, use the Helmholtz equation.

$$[\nabla^2 + \omega^2 \mu_o \varepsilon_o] E_z = 0 \tag{2.9}$$

This equation admits solutions of the form

$$E_z = E_o \left\{ \begin{matrix} \sin \beta_x x \\ \cos \beta_y y \end{matrix} \right\} \left\{ \begin{matrix} \sin \beta_y y \\ \cos \beta_y y \end{matrix} \right\} \quad [8] \tag{2.10}$$

where only one solution in each of the brackets must be selected. (Note also that the variation with z has again been dropped because of the thinness of the cavity in the z direction.) To determine which solutions to select, consider the boundary conditions

$$E_z (x, 0, 0) = 0 \tag{2.11}$$

$$E_z (0, y, 0) = 0 \tag{2.12}$$

$$E_z (-a, y, 0) = 0 \tag{2.13}$$

$$H_x (x, b/2, d) = 0 \tag{2.14}$$

It is apparent from the first two boundary conditions that the only admissible solution for E_z is

$$E_z = E_o \sin \beta_x x \sin \beta_y y \tag{2.15}$$

From the third boundary condition, it is clear that $\sin \beta_x (-a) = 0$ or

$$\beta_x = \left(\frac{m\pi}{a}\right) \tag{2.16}$$

Now, the magnetic field can be calculated from (2.8)

$$H_x = \frac{-\beta_y}{j\omega\mu_o} \left[E_o \sin (\beta_x x) \cos (\beta_y y)\right] \tag{2.17}$$

The fourth boundary condition states that $H_x (x, b/2, d) = 0$. Therefore,

$$\beta_y \, b/2 = \frac{n\pi}{2} \; ; \; n \text{ odd}$$

or
$$\beta_y = \left(\frac{n\pi}{b}\right) \; ; \; n \text{ odd} \tag{2.18}$$

Substituting (2.16) and (2.18) into (2.15) yields

$$E_z = E_o \sin\left(\frac{m\pi x}{a}\right) \sin\left(\frac{n\pi y}{b}\right) \tag{2.19}$$

Substituting (2.19) into (2.9) and solving for $\omega^2 \mu_o \varepsilon_o$ give

$$\omega^2 \mu_o \varepsilon_o = \left(\frac{m\pi}{a}\right)^2 + \left(\frac{n\pi}{b}\right)^2 \tag{2.20}$$

which is the dispersion relation for the modified cavity. Solving (2.20) for ω yields

$$\omega_{mn} = \frac{1}{\sqrt{\mu_o \varepsilon_o}} \left[\left(\frac{m\pi}{a}\right)^2 + \left(\frac{n\pi}{b}\right)^2\right]^{1/2} \tag{2.21}$$

which is the resonant frequency for the mn mode of this modified cavity.

Rewriting some of the important equations for the modified cavity:

$$E_z = E_o \sin\left(\frac{m\pi x}{a}\right) \sin\left(\frac{n\pi y}{b}\right) \tag{2.22}$$

$$H_x = \frac{-n\pi/b}{j\omega\mu_o} \left[E_o \sin\left(\frac{m\pi x}{a}\right) \cos\left(\frac{n\pi y}{b}\right)\right] \tag{2.23}$$

$$\omega_{m,n} = \frac{1}{\sqrt{\mu_o \varepsilon_o}} \left[\left(\frac{m\pi}{a}\right)^2 + \left(\frac{n\pi}{b}\right)^2\right]^{1/2} \tag{2.24}$$

Note that these three equations for the modified cavity are of the same form as (2.1), (2.2) and (2.4a) for the closed cavity of Figure 2. In fact, (2.24) and (2.4a) are exactly alike. Thus, a cavity can be created that is one half as wide as the closed cavity of Figure 2 (and still have

the same resonant frequency) by extending a slot across the top of the cavity as shown in Figure 5. This is an extremely encouraging result because it means that an array of modified cavity antennas (of the type in Figure 5) can be built in about half the space of the previous arrays which used unmodified cavities (of the type in Figures 1 and 3). The antennas tested during this research were all designed in accordance with Figure 5 for a specific resonant frequency as given by (2.24).

2.3 Cavity Construction

In general, the prototype cavities were constructed by milling 1/16" deep into a 1/8" brass sheet. The length and width of the cavities were determined by Eq. (2.24) with $m = n = 1$ since we are interested in using the TM_{110} mode. The radiating slot was cut along the length of one edge of the cavity. At this point, the sides, top and radiating slot (in the top of the cavity) were completed. The bottom of the cavity was a sheet of double clad 1/16" Rexolite ($\varepsilon_r = 2.6$) fastened to the cavity body by brass screws tapped into the 1/8" brass. Figure 6 illustrates an exploded view of the completed antenna.

2.4 Aperture Coupling

To turn this slotted cavity into an antenna, energy must somehow enter into the cavity and be radiated out the radiating slot in the top. In the past, this was usually done by either inserting a probe in the bottom of the cavity, or running a microstrip line across the radiating slot as Szmurlo did (see Chapter 1). Instead of using one of these traditional

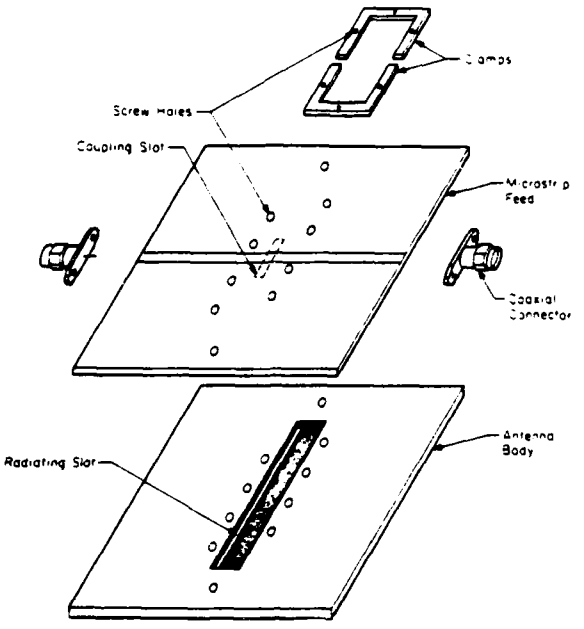

Figure 6. Exploded view of completed antenna.

methods to feed these cavities, a new approach was used: aperture coupling. In aperture coupling, one side of the double-clad Rexolite is the cavity bottom. On the other side, the copper cladding is peeled away except for a strip of a specific width (4.4 mm for 50Ω in 1/16" Rexolite) which acts as the antenna feedline. On the cavity bottom side, a narrow, short strip of copper orthogonal to the feedline (which is on the other side) is peeled away to form the coupling aperture (or coupling slot). An example of an aperture coupled cavity-backed slot is shown in Figure 7. Aperture coupling has some advantages over the more traditional methods of feeding the cavity. For one thing, it is a flatter system of feeding the antenna than probe feeding and thus is better suited for conformal mounting. Additionally, aperture coupling does not interfere with the radiation of energy through the radiating slot. When the same slot is used for both coupling and radiation, this interference (scattering from

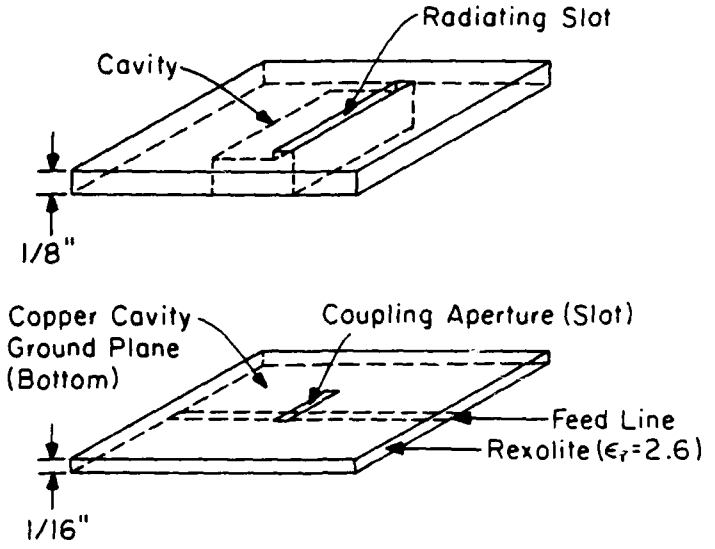

Figure 7. Aperture coupled cavity-backed slot antenna.

the feedline) is unavoidable. With aperture coupling, the feedline can be placed anywhere along the slot (not just the center) without affecting the antenna patterns. Finally, aperture coupling offers a new degree of freedom, variation of the coupling aperture size, not available heretofore. On the other hand, when aperture coupling is used, some radiation will leak out the coupling aperture. Thus, power gain may be lower when aperture coupling is used.

Aperture coupled antennas are relatively new devices. Pozar [9] first proposed the concept for exciting microstrip patch antennas in 1985. Since then he and others, notably Sullivan and Schaubert [10], have investigated, with some success, the use of aperture coupling with simple microstrip patch antennas. However, until now, aperture coupling has not been used to drive cavity-backed slot antennas.

CHAPTER 3
PROTOTYPE 1

In this chapter, the first prototype antenna and initial testing will be discussed. Four prototypes were constructed and tested: one that was the same size as the largest cavity in the array (Prototype 1), one the same size as the smallest cavity in the array (Prototype 2) and two others in between the largest and smallest cavities (Prototypes 3 and 4). The testing on Prototype 1 was by far the most conclusive. The results of various tests on this prototype were used to establish the length and position on the cavity bottom of the coupling slot as well as the antenna array scaling factor (τ). Testing on Prototypes 2 and 3 had some unexpected results, which will be discussed in the next chapter.

3.1 Prototype 1 Construction

Prototype 1 was built to the specifications of Figure 5 with a = 10 9/16" (26.829 cm), b/2 = 1 17/32" (3.889 cm), and W_s = 5/32" (0.3969 cm). The cavity bottom/feedline was constructed of 1/16" Rexolite (ε_r = 2.6). On the feedline side, all the copper except a narrow strip (the feedline) was removed. The width of the strip (4.4 mm) was determined by formulas proposed by Edwards [11] for the given height (1/16") and a characteristic impedance of 50 ohms. SMA connectors were attached to each end of the line. The line was tested on a TDR and trimmed for a good match. The coupling aperture was then cut in the middle of the other side of the Rexolite with the arbitrarily selected width of 2.5 mm and length 11.45 cm. The length of the coupling slot was easily varied by covering portions of the 11.45 cm opening with copper tape. The position of the coupling slot

in the cavity bottom was also variable by simply loosening the connecting screws and sliding the cavity bottom in either direction.

To determine the resonant frequency of this cavity, its dimensions were substituted into Equation (2.24). This substitution resulted in a resonant frequency of 12.615×10^9 rad/s or 2 GHz. For a closed cavity of these dimensions, a resonant frequency of 2 GHz would be expected. But, in fact, (2.24) assumes that $W_s = 0$ (which it is not) and does not take into account the coupling aperture. Therefore, it was expected that the actual resonant frequency of Prototype 1 would be proportionally less than 2 GHz with the increase in size of the apertures.

3.2 Prototype 1 Testing Procedure

To test Prototype 1, and the other prototypes as well, the following sequence of steps was followed using the HP 8510 Network Analyzer.

1) Using the calibration kit, a calibration over the frequency range of interest was executed.

2) The measurement plane was then shifted to coincide with the coupling aperture. For reflection measurements, this was accomplished by using a reference short. The short was constructed similar to the microstrip feed line except it was only half as long and had a shorted plane on one end. Thus, the electrical distance between the shorted plane and the connector was equal to the electrical distance between either connector and the coupling slot of the microstrip feed line. The short was connected to the HP 8510 and electrical delay and phase

offset were added until the trace (S_{11}) on the 8510 collapsed to a point at the left edge of the Smith chart on the real axis. Similarly, electrical delay and phase offset were added to transmission measurements via a reference 'thru' (which was the cavity bottom/feed line with the coupling aperture covered with copper tape).

3) Finally, the antenna itself was connected to the 8510 (with the values of electrical delay and phase offset gained through step 2 above programmed into the 8510) as a two-port device and measurements recorded of S_{11} and S_{21}.

3.3 Advantages of Aperture Coupling

Once the first two steps were completed for the cavity bottom/feed line and cables (from 8510 to antenna), numerous measurements as described in step three were made with the length and position of the coupling aperture as variables. As expected, the longer the coupling slot, the lower the resonant frequency (as indicated by a crossing of the real axis by S_{11}). Furthermore, as the coupling slot was shortened, the size of the S_{11} locus shrunk toward the center of the chart. The impact of this phenomenon can best be seen by comparison of Prototype 1 data with Szmurlo's single cavity data. Figure 8a is the S_{11} data for Szmurlo's Cavity 6. Note the similarity between the shape of the locus in Fig. 8a and that of Fig. 8b, the S_{11} data for Prototype 1 with a coupling slot length of 11.45 cm. Neither Szmurlo's Cavity 6 nor Prototype 1 (in this configuration) is a very well-matched radiator (as evidenced by the large distance between the center of the chart and the crossover point on the real axis at resonance).

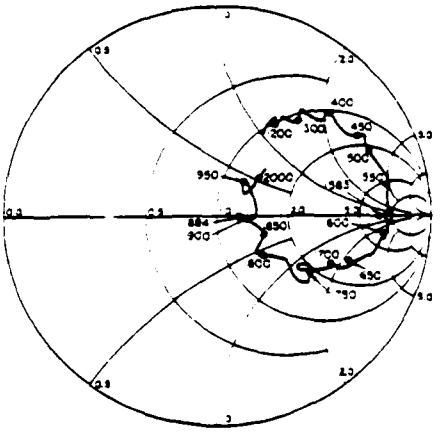

Figure 8a.
S_{11} - Szmurlo's cavity 6 [5].

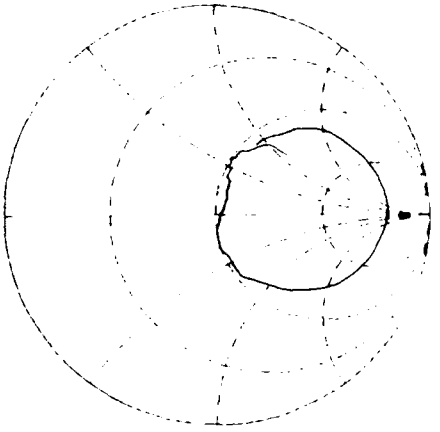

Figure 8b.
S_{11} - Prototype 1,
coupling slot length = 11.45 cm.

Figure 9 shows the S_{11} and S_{21} locus for Prototype 1 with the much shorter coupling slot length of 4.5 cm. Note that the S_{11} locus of this figure indicates a much better match than the antennas of Figure 8. This ability to affect the antenna impedance by varying the length of the coupling slot is exciting because it gives the antenna engineer a degree of freedom not previously available. Conversely, the position of the coupling slot had virtually no effect on the resonant frequency or the shape of the S_{11} and S_{21} loci.

3.4 Prototype 1 Data and Analysis

As stated earlier, the purposes of testing the first prototype included determining the optimum length of the coupling aperture and the optimum scaling factor for the log-periodic array. The performance factor

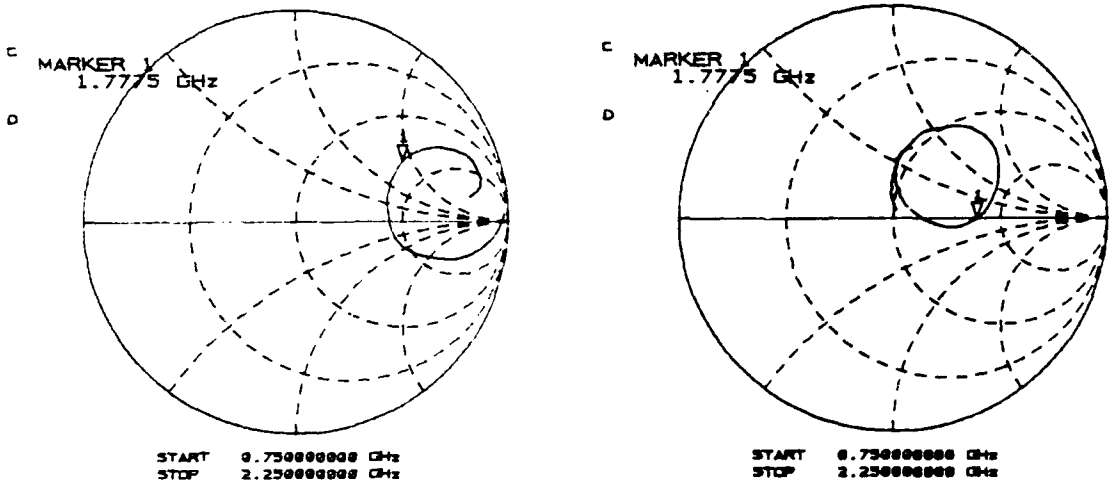

Figure 9. S_{11} and S_{21} - Prototype 1, coupling slot length: 4.5 cm, coupling slot position: against cavity wall opposite radiating slot.

that was used to determine the optimum was the upper bound on the radiation efficiency as defined by

$$e_R = 100 \left[\frac{1 - |S_{11}|^2 - |S_{21}|^2}{1 - |S_{11}|^2} \right] \quad \% \tag{3.1}$$

A close look at this equation reveals that the numerator represents the part of the signal that is neither reflected nor transmitted; this is the portion of the signal that is radiated (discounting losses). The denominator, on the other hand, represents the portion of the signal that is not reflected; this is the sum of the radiated and transmitted portions of the signal. Hence, (3.1) could be rewritten as

$$e_R = 100 \left[\frac{\text{radiated}}{\text{radiated + transmitted}} \right] \quad \% \tag{3.2}$$

Thus, e_R is the percentage of the signal remaining after reflection that is radiated. It was decided that a radiation efficiency at resonance of around 60% would be best for application to a log-periodic array. The reason is that no single element in the array should radiate so much of the signal that there would not be enough signal left to excite remaining elements. If $e_r \gg 60\%$, the active region of the array would be made up of just one or two elements.

With this in mind, the data from Prototype 1 testing were examined to see how the efficiency changed as a function of the coupling slot length. As expected, the efficiency declined as the length of the coupling slot shortened, most likely because less energy is coupled into the cavity as the coupling slot becomes shorter. The antenna performance with the three specific coupling slot lengths that yielded an efficiency of around 60% was then closely scrutinized. Table 3.1 lists the parameters of interest of these three configurations.

TABLE 3.1

PROTOTYPE 1 - PARAMETERS OF INTEREST

Coupling Slot Length (cm)	Resonant Freq. (GHz)	e_R (%)
5	1.655	72.38
4.5	1.78	53.643
4	1.86875	50.64

To determine which of these three coupling slot lengths to choose, and to simultaneously determine the scaling factor, a power distribution analysis much like that done by Tammen for his log-periodic array of monopole-slot elements was performed [4]. The goal of this analysis was to determine how power would be distributed among the elements of the log periodic array at different frequencies for a given scaling factor (and in our case, a given coupling slot length). With this result a scaling factor can be selected which, for a given frequency, will produce an adequate number of elements with relative power above a desired threshold. The elements above the threshold will be those that make up the active region of the antenna for that frequency.

In a nutshell, the analysis consists of creating an efficiency versus frequency curve for each cavity in the array. Then, for a given frequency, the e versus f curve of the smallest cavity can be used to determine what percentage of power incident on this first cavity will be radiated. Next, the e versus f curve for the second smallest cavity is used to determine what percentage of the remaining power is radiated by this second cavity, and so on. Since it was too difficult to generate an e versus f curve for each cavity, it was assumed that the curves for all the cavities had the same shape. To obtain an e versus f curve for the higher frequency cavities, the frequencies of the e versus f curve for Prototype 1 were simply scaled. For individual log-periodic elements, one could expect this scaling to be accurate. The fact that the cavity depths in our array are not log-periodically scaled should have little impact. Mayes found that efficiency versus frequency characteristics for shallow cavities did not change much with small changes in cavity depth [12].

A methodical example will serve to more clearly explain the analysis described above. For this example a coupling slot length of 4.5 cm and a scaling factor of $\tau = 0.92$ was used. The steps in the analysis follow:

1) Generate an efficiency versus frequency curve for the configuration of interest (e.g., Prototype 1 with a coupling slot length of 4.5 cm) using $|S_{11}|$ and $|S_{21}|$ from the HP 8510 and Equation (3.1). Figure 10 shows the curve generated for this example.

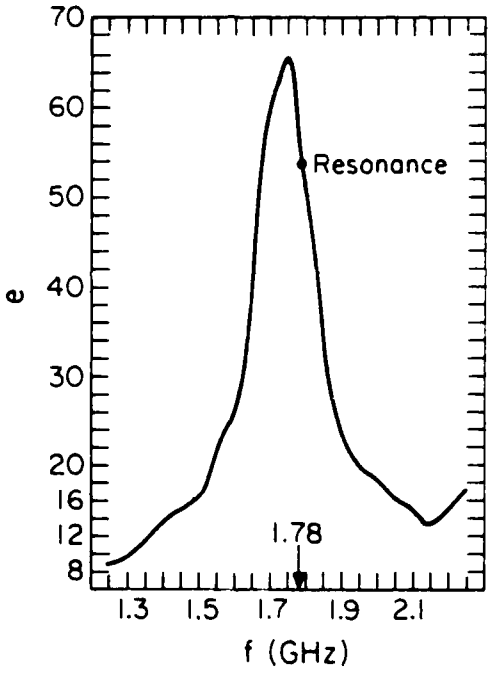

Figure 10. Efficiency versus frequency; coupling slot length = 4.5 cm.

2) Determine the number of cavities, n, in the required array bandwidth. Since an electrical bandwidth of 5:1 was desired, it was felt that a structural bandwidth of 6:1 was needed. To achieve a 6:1 structural bandwidth with $\tau = 0.92$ indicates that for any

dimension X_o, of the largest element, the smallest element will have that dimension equal to 6 X_o $(0.92)^m$, i.e.,

$$6\ X_o\ (0.92)^m = X_o$$

$$0.92^m = 1/6$$

$$m = \frac{\log\ (1/6)}{\log\ (0.92)} = 21.489$$

= number of other elements

in addition to the first element. Therefore, 22 elements were needed to achieve a 5:1 electrical bandwidth with a scaling factor of 0.92. A drawing of such an array is shown in Figure 11.

3) Generate a power distribution table (see Table 3.2).

a) Translate a particular frequency of interest by multiplying it by $(0.92)^m$ (where m is the exponent referred to in Figure 10). Start with the highest m in the array and continue to change m until the translated frequency (f_t) is greater than or equal to 1.25 GHz, the lowest frequency of Figure 9. (Alternatively, solve $m = \log\ (\frac{\text{freq of interest}}{1.25\ \text{GHz}})\ /\ \log(0.92)$ and round up to find the highest m which yields a translated frequency above or equal to 1.25 GHz.)

b) From Figure 9, find the value of e corresponding to f_t and place it in a table (e.g. Table 3.2) where f and m intersect.

c) To find the fractional power for the m-1 element, use the following formula from Tammen [4]

$$FP_i = e_i\ [100 - \sum_{n=1}^{i-1} FP_n]$$

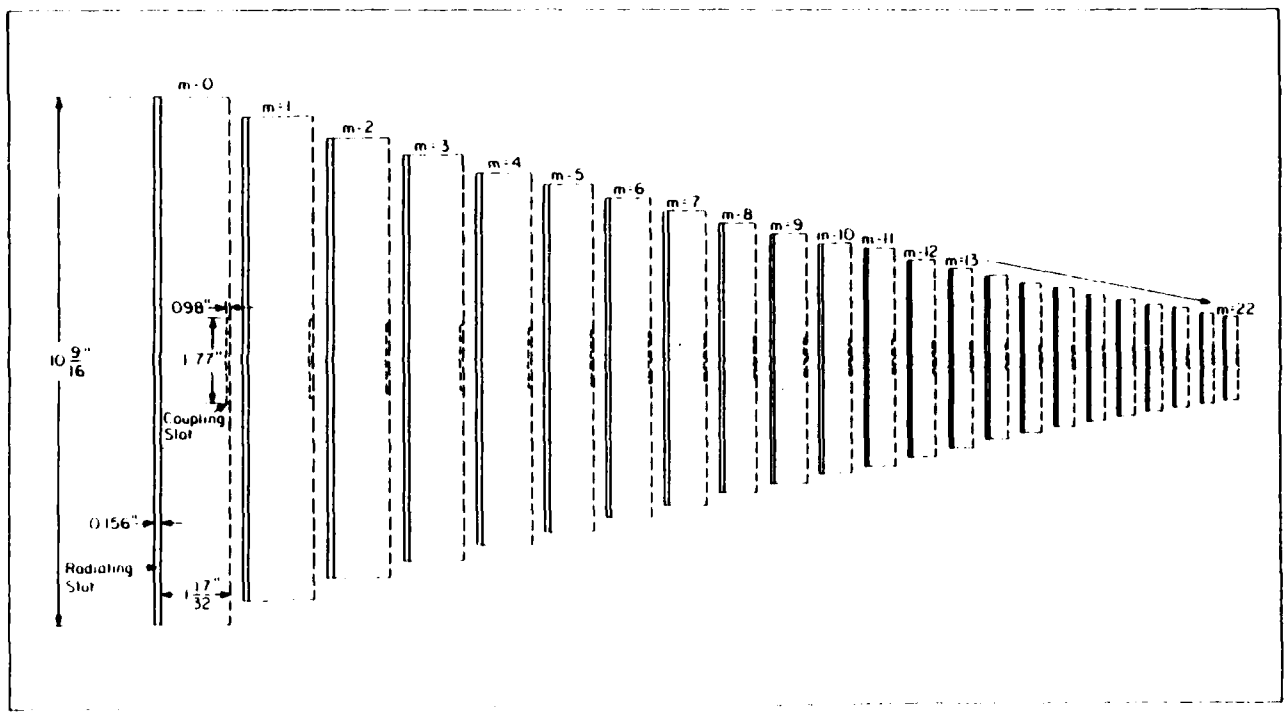

Figure 11. Antenna array with $\tau = 0.92$. To determine size of smaller cavities, multiply dimensions of right-most cavity by $(0.92)^m$.

TABLE 3.2

POWER DISTRIBUTION AMONG ARRAY ELEMENTS
$\tau = 0.92$
COUPLING SLOT LENGTH = 4.5 cm

element (m) / f (GHz)	22	21	20	19	18	17	16	15	14	13	12	11	10	9	8	7	6	5	4	3	2	1	0
1.5																					9.2	10.4	12.9
2.0																		12.0	12.76	13.17	24.8	23.8	2.42
2.5															9.8	10.01	12.5	15.4	32.88	7.25	2.12	1.41	
3.0													9.78	12.55	13.20	18.7	29.75	4.65	2.05	1.26			
3.5											9.5	11.58	12.23	17.33	30.6	7.13	2.15	1.27					
4.0										11.247	13.577	16.54	32.25	12.66	2.7								
4.5								9.5	11.765	12.20	17.29	30.53	6.67	2.23	1.32								
5.0							10.5	12.978	13.238	25.31	24.301	3.55	1.67										
5.5						10.5	12.978	11.86	29.74	18.73	3.56	2.07											
6.0					10.9	13.63	17.36	32.542	12.27	2.66													
6.5				10.5	12.978	15.305	37.3	12.807	2.43														
7.0		10.2	17.062	27.64	23.902	5.34	2.61																
7.5		9.78	12.548	12.816	18.81	29.701	4.90	2.06															
8.0	9.0	10.92	12.412	16.917	30.70	7.22	2.44	1.48															
8.5	11.5	13.496	17.4	32.83	11.15	2.642	1.692																
9.0	14.8	18.24	30.13	19.52	3.8	2.19	1.75																
9.5	17.0	26.56	37.21	5.00	2.39	1.66																	
10.0	25.992	45.89	10.03	3.35																			
10.5	55.00	22.97	4.4																				

where FP_i is the fractional power of the ith element, FP_n is the fractional power of the nth element and e_i is found from Figure 9 by using f_t/τ.

d) Repeat previous steps until the whole line for the frequency of interest is filled in (see Table 3.2).

Once the previous steps are completed over a range of frequencies, the power distribution table can be completed. Several tables for different scaling factors and different coupling slot lengths were created in this manner. Based on previous research, it was decided the active region for a given frequency needed to have at least three elements with relative power above 10. The table with the greatest bandwidth of frequencies that had three or more elements with relative power above 10 was selected. That table corresponded to a τ of 0.92 and a coupling slot length of 4.5 cm. It is reproduced in this report as Table 3.2.

3.5 Conclusions from Prototype 1 Testing

Many valuable things were learned from testing Prototype 1. First of all, the data verified the theory of bisecting the traditional rectangular CBS. Second, the 'optimum' coupling slot length for Prototype 1 was selected via power distribution analysis. Finally, and most importantly, a new benefit of using aperture coupling was realized. That is, the performance of the prototype antenna (and presumably the performance of the entire array) can be controlled, in part, by the length of the coupling slot.

CHAPTER 4
OTHER PROTOTYPES

It was decided that a second prototype should be built and tested in order to see if scaling the antenna altered the performance parameters observed for Prototype 1. This second prototype was designed to have the same dimensions as the smallest element of the antenna array. Based on the theory of scaling, its resonant frequency was expected to be approximately 11 GHz, an order of magnitude higher than any previously tested CBS antenna. Since the wavelength shrinks proportionally as the frequency rises, much greater attention to detail was used when constructing and testing this higher frequency device than was used when building and testing Prototype 1. Nevertheless, problems were anticipated and a major problem was encountered during preliminary testing of Prototype 2.

The basic problem was that the impedance locus of S_{11} moved in a counterclockwise (instead of clockwise) direction as frequency increased (Fig. 12a). Interestingly, the S_{21} locus (Fig. 12b) was normal (clockwise). When further testing of Prototype 2 did not reveal the cause of the anomaly, a third prototype with a resonant frequency intermediate to those of Prototypes 1 and 2 (f_r = 7.35 GHz) was constructed and tested. Unfortunately, Prototype 3 also manifested the unexplained phenomenon. A fourth prototype with a resonant frequency still lower than that of Prototype 3 was constructed and tested (f_r = 3.77 GHz); the problem was not observed for this final prototype. Eventually, the cause of this frequency-related phenomenon was discovered. This chapter will detail the problem, the steps taken in search of the cause, the cause, and the solution to the problem.

4.1 The High Frequency Anomaly

Recall from Prototype 1 data (Figure 9) that both the S_{11} and S_{21} loci travel clockwise (CW) around the Smith Chart as frequency increases.

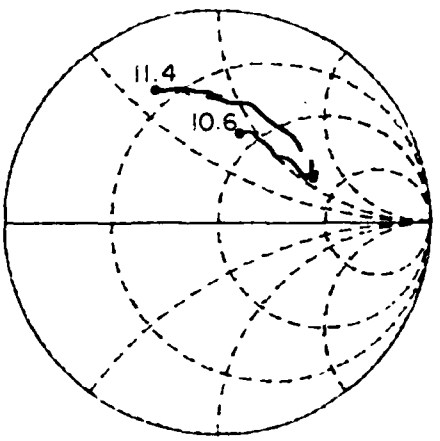

Figure 12a. S_{11} - Prototype 2. (10.6 - 11.4 GHz)

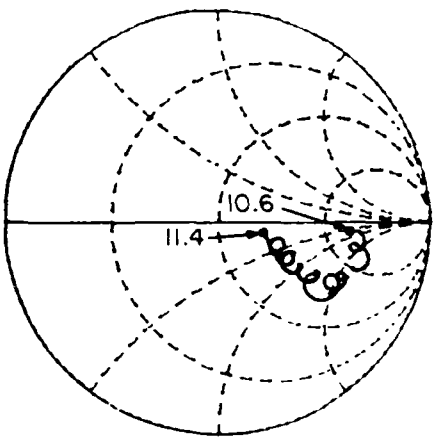

Figure 12b. S_{21} - Prototype 2. (10.6 - 11.4 GHz)

The reason for this clockwise progression can be found in Foster's Reactance Theorem (FRT). This theorem states: "The slope of the reactance or susceptance for a loss-free one-port is always positive" [13]. Granted, by design an antenna is not lossless and those discussed here are two-ports. However, until Prototype 2 was tested, no antennas had ever seemingly violated this theorem.

4.1.1 Determining the cause

As can be seen from Figure 6, the prototypical CBS antenna has very few components. It was decided, therefore, to change/alter different components of the antenna (one at a time) and observe the effect on the S_{11} trace. First, the metal clamps that held the microstrip feed in place were replaced with plexiglass clamps. As Figure 13 illustrates, this change had no effect.

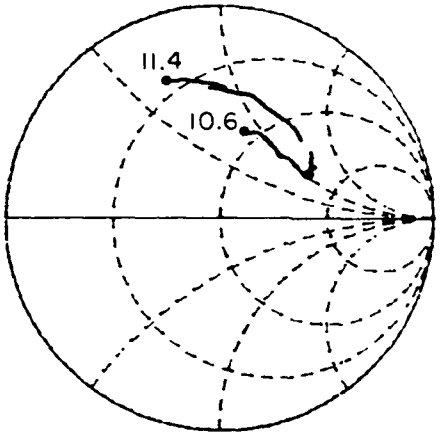

Figure 13. S_{11} - Prototype 2 with plexiglass clamps. (10.6 - 11.4 GHz)

Next, the radiating slot was made more shallow. This change shifted the location of the trace, but not the shape of it (Figure 14).

Before making any further changes, Prototype 3 was built to determine if this anomaly was also observed at slightly lower frequencies. As mentioned earlier, Prototype 3 also displayed the counterclockwise phenomenon (Figure 15). It was then hypothesized that perhaps losses were responsible

for this effect and, therefore, an effort was made to reduce them wherever possible. The first step in this direction was to replace the dielectric

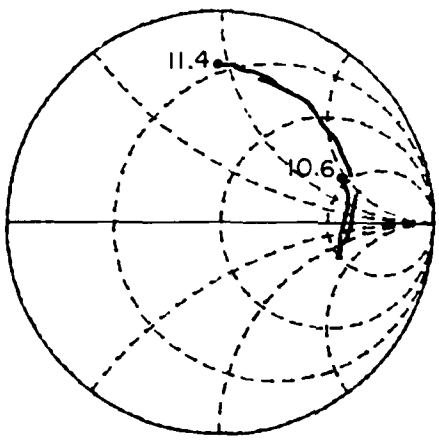

Figure 14. S_{11} - Prototype 2 with shallower slot. (10.6 - 11.4 GHz)

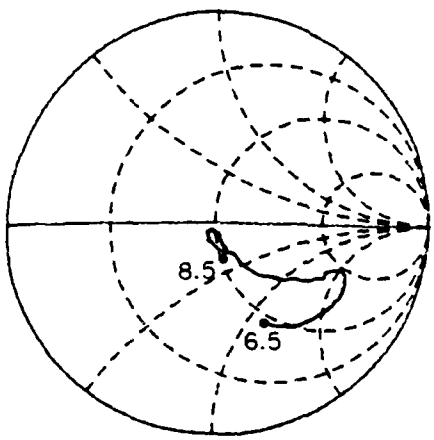

Figure 15. S_{11} - Prototype 3. (6.5 - 8.5 GHz)

in the prototype with a much thinner one (15 mils). In addition to reducing losses, this step was also taken to make sure that a quasi-TEM mode was still being propagated on the microstrip line, because as frequency rises, the microstrip height must shrink to ensure quasi-TEM propagation [11]. These modifications, however, had no impact on the counterclockwise phenomenon (Fig. 16). To lessen losses still more, the RG-214 cables used as test port extensions from the 8510 to the antenna under test were replaced

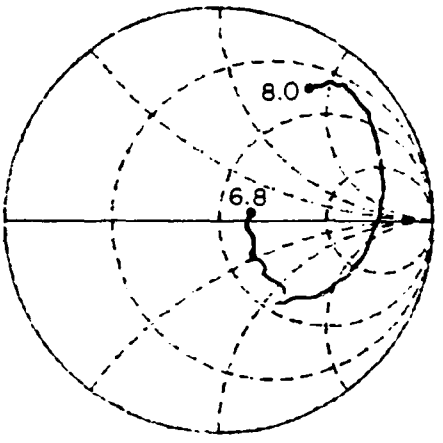

Figure 16. S_{11} - Prototype 3 with 15 mil thick microstrip feed. (6.8 - 8 GHz)

with precision semirigid cables. Although the S_{11} locus measured following this modification indicated less loss, it still proceeded counterclockwise with frequency. Again attempting to maximize performance and reduce loss, the connectors on the antenna were replaced by a myriad of different higher precision connectors. These changes had no effect on the problem.

Since alteration of virtually every antenna component had no impact on the direction of the S_{11} locus, it was concluded that something outside the antenna was the cause of the anomaly. Therefore, a closer examination of the reference through (which also acts as the microstrip feed) and reference short were made. In addition to the usual examination on the Time Domain Reflectometer (TDR) mode of the 8510, the return loss of the through and short was checked over a very wide bandwidth (0.0896 - 18.0 GHz). This was done because it was discovered that poorly matched lines often exhibit perturbations in their return loss plots above a certain frequency. Figure 17 shows the TDR plot and return loss for a typical poorly matched microstrip line and the associated return loss plot. The hypothesis was that these perturbations indicated the propagation of higher-order modes which could

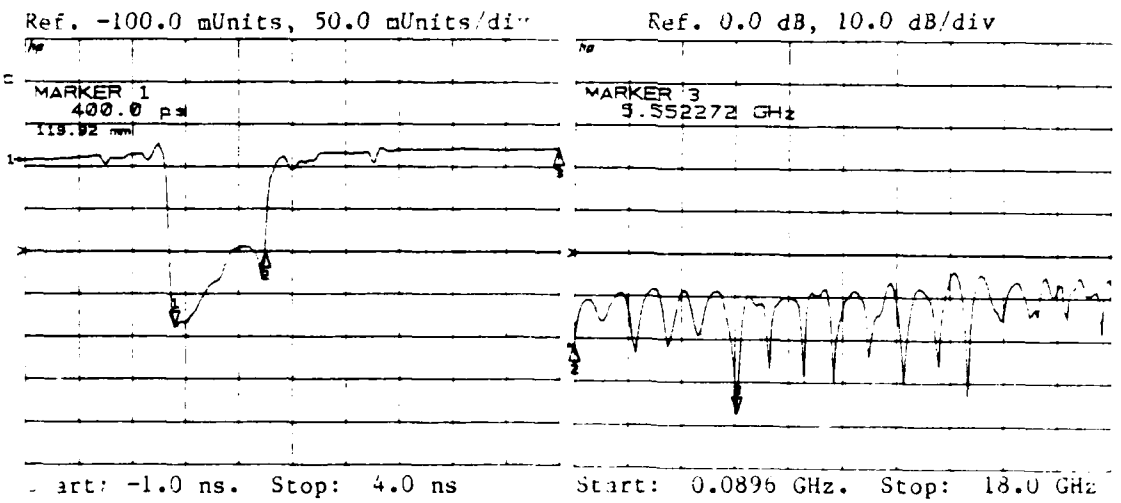

Figure 17a.
TDR - Poorly matched line.

Figure 17b.
Return loss - Poorly matched line.

cause the S_{11} locus to behave abnormally. Although this hypothesis was never confirmed during this research, the return loss plots did reveal

something interesting which ultimately pointed to the cause of the unusual S_{11} loci.

The return loss plot for the through (Fig. 18) had no perturbations throughout the frequency range. This indicated the transmission line was probably not the source of the problem. The return loss plot of the short, however, was extremely abnormal. A short should have zero return loss for

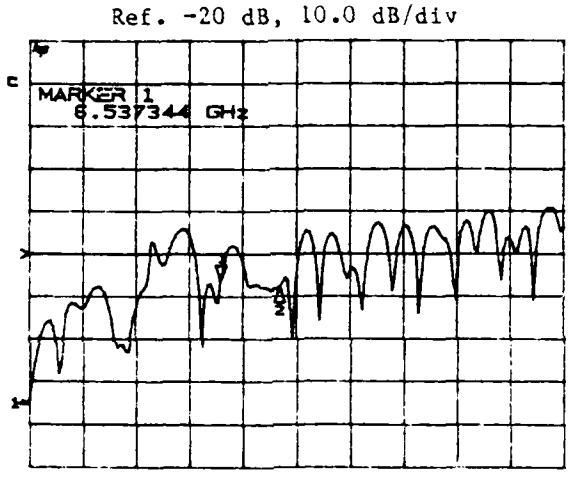

Figure 19. Return loss - Through.

all frequencies because $|\Gamma|$ for a short is one. Although the reference short for Prototype 3 had the TDR plot of a good short (Fig. 19a), its return loss was not zero for all frequencies (Fig. 19b). In fact, there were a number of frequencies where its return loss was substantially less

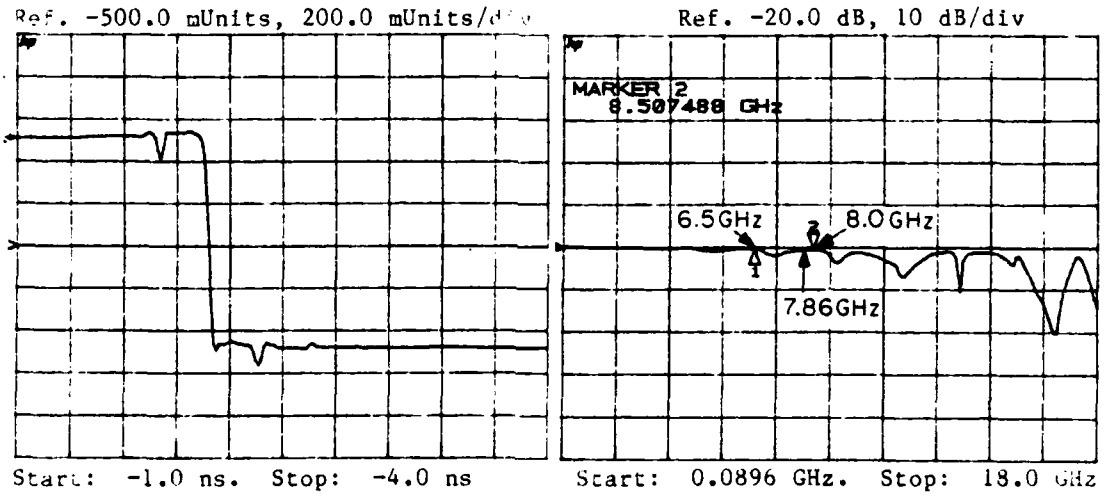

Figure 19a.
TDR - Reference short.

Figure 19b.
Return loss - Reference short.

than zero. Note the two markers in Figure 19. They indicate the frequency range within which Prototype 3 was tested. Figure 20a shows the S_{11} locus for the third prototype when the measurement plane was established using the short of Figure 20b (Figure 19b repeated). The plot of Figure 20a is initially moving counterclockwise and then begins moving clockwise at about 7.8 GHz. In other words, the locus is abnormal from 6.5 - 7.8 GHz. A close examination of Figure 20b reveals that 6.5 - 7.8 GHz is the same range (within the 6.5 - 8 GHz band of Figure 20a) in which the return loss of the reference short is not equal to zero.

It was concluded, therefore, that the cause of the backward phenomenon was the inconsistency of the reference short in the frequency range of interest. Consequently, the measurement plane was also inconsistent

because the inconsistent reference short was used to establish its location. Simply put, the measurement plane for the reflection measurements

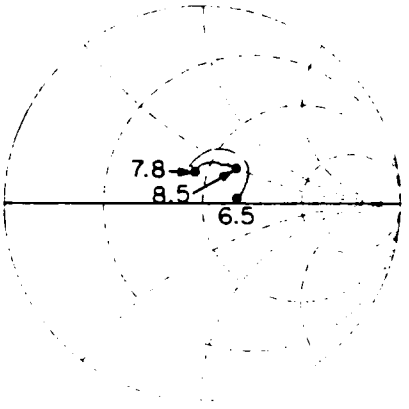

Figure 20a.
S_{11} - Prototype 3.

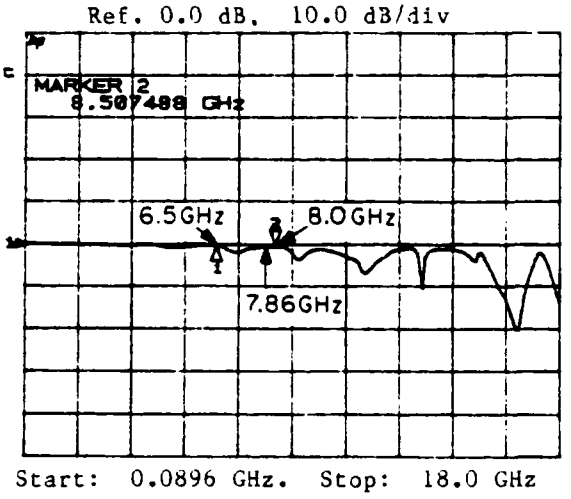

Figure 20b.
Return loss - Reference short.

was changing with frequency. This explanation also accounts for the fact that all of the transmission measurement plots (S_{21}) were normal.

Although the evidence already discussed was convincing, a different method of establishing the measurement plane had to be established and the effect of the new method on the S_{11} trace observed to validate the theory. Recall that the microstrip feed network doubled as the reference through and the coupling aperture was exactly in the middle of it. Thus, the electrical delay and phase offset we had established for the transmission measurements could also be used to establish the reference plane for the reflection measurements. This procedural modification was tested, and the resulting S_{11} locus did indeed move in the right (clockwise) direction.

4.2 Further Testing of Prototypes 2, 3, and 4

The discovery of the cause of this anomaly allowed the research to move forward but the performance factors of the first two prototypes were never correlated because of equipment breakdowns and parts shortages. Since time was limited, it was decided to hypothesize that the performance factors would indeed correlate and to pursue the design, construction and testing of the antenna array.

CHAPTER 5
LOG-PERIODIC ARRAY OF APERTURE-COUPLED CAVITY-BACKED SLOTS

The design of the log-periodic elements was accomplished by multiplying the dimensions of Prototype 1 by τ^m ($\tau = 0.92$; m is defined in Figure 11). Two dimensions, however, were not scaled: the cavity depth and the separation between adjacent cavity walls. The cavity depth was not scaled in order to make construction of the array easier. Furthermore, as stated in Chapter 3, earlier research by Mayes indicated that variation in the depths of shallow cavities had little effect on their performance parameters; therefore, no impact was expected from this subtle deviation from true log-periodic design. Conversely, the separation distance between antenna elements was not the result of a decision based on previous research and theory; it was a design flaw. Fortunately, the data presented in this chapter indicate that this design flaw had little, if any, effect on the frequency-independent performance of the antenna, although it did impact the design of the feeder and thereby limit the bandwidth of the antenna.

The array elements were milled out of 1/8" brass to the specifications of Figure 11. The array feed network was constructed in the same manner as the prototype feedlines using 1/16" double clad Rexolite. However, the feed network for the array was designed much differently than were the prototype feedlines. This chapter focuses on the design and construction of the array feed network, the measurement of the scattering parameters, and the antenna patterns of the antenna array.

5.1 Feed Network/Cavity Bottom Design and Construction

The design of the feed network was in large part dictated by the goal of having an antenna array that produced a backfire radiation pattern. To

achieve backfire radiation, the waves radiated by the antenna elements must add in phase in the backfire direction. One successful method of obtaining this in-phase addition of radiated waves has been to ensure that the phase shift going from one element to another and back is equal to 2π radians [5]. In the case of this antenna array, the total phase shift is equal to that of the incident wave as it travels along the feedline from the coupling slot of one element to that of the next plus that of the radiated wave as it travels in free space back to the radiating slot of the first element. If the feedline followed a straight path between coupling slots, this phase shift would be less than 2π. Therefore, excess feedline, of length d, must be added between coupling slots. Analytically, a formula for d can be derived as follows:

$$\beta_o d_s + \beta d = 2\pi \text{ radians (phase difference} \tag{5.1}$$

equivalent to d_t = one wavelength)

$$d = \frac{2\pi - \beta_o d_s}{\beta} = \frac{2\pi - \beta_o d_s}{\sqrt{\varepsilon_r}\ \beta_o}$$

$$= \frac{1}{\sqrt{\varepsilon_r}} \left(\frac{2\pi}{\beta_o} - d_s\right) = \frac{1}{\sqrt{\varepsilon_r}} \left(\frac{2\pi c}{\omega} - d_s\right)$$

Therefore $$d = \frac{1}{\sqrt{\varepsilon_r}} \left(\frac{c}{f_r} - d_s\right) \tag{5.2}$$

In Equation (5.2), d_s is the physical distance between the radiating slots, ε_r is the relative permittivity of the dielectric substrate of the feed network, c is the speed of light in free space, and f is the resonant frequency (as defined by scaling resonant frequency of Prototype 1) of the smaller of the two cavities.

If an infinite front-to-back ratio were desired, the feedline length would be designed so that the waves radiated in the direction of the incident wave on the feedline would be 180 degrees out of phase. Because of time limitations, an infinite front-to-back ratio was not one of the goals of this research.

The resultant section of line between any two coupling slots would have a displaced portion and a main-line portion as in Figure 21.

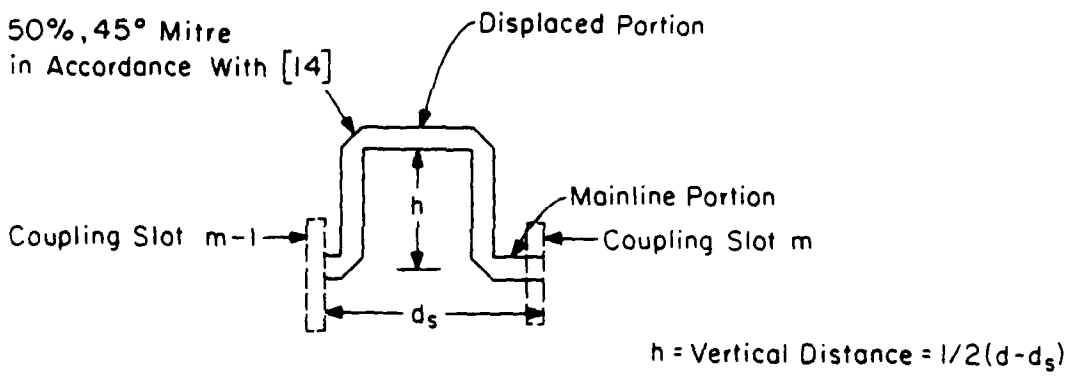

Figure 21.

Section of meandering line between two coupling slots.

The whole feed network for the 23 cavity array was to be built using the design shown in Figure 21, but another problem arose. At higher frequencies (> 4.2 GHz), the distance, h, shrinks so much that the displaced portion and the main-line portion of the feedline begin to blend together. As the frequency continues to climb, h would eventually have to be a negative quantity in order for Equation (5.1) to be satisfied. This fact presents a problem because a negative distance is not physically realizable.

This problem is a result of the design flaw discussed in paragraph one of this chapter. If the antenna did not have this flaw, then the distance h of any given element would always be the scaled h of the previous element. To see this, rewrite Equation 5.2 and consider the distance d_m between the elements m and m-1 of a correctly scaled array.

$$d_m = \frac{1}{\sqrt{\varepsilon_r}} \left(\frac{c}{f_{rm}} - d_{sm}\right) \tag{5.3}$$

where f_{rm} is the resonant frequency of element m, and d_{sm} is the distance between elements m and m-1. Equation (5.3) can then be written to include the scaling factor as follows:

$$d_m = \frac{1}{\sqrt{\varepsilon_r}} \left[\frac{c}{(f_{ro})/(0.92)^m} - (d_{so})(0.92)^m\right]$$

$$d_m = \frac{1}{\sqrt{\varepsilon_r}} \left[(\lambda_o)(0.92)^m - (d_{so})(0.92)^m\right]$$

$$d_m = \frac{(0.92)^m}{\sqrt{\varepsilon_r}} \left[\lambda_o - d_{so}\right] \tag{5.4}$$

where the parameters with zero in the subscript are parameters of the largest (m=0) element. From Equation (5.4) it is apparent that d_m (and thus $h = d_m - d_{sm}$) for any given element is d_{m-1} (0.92). In other words, both d_m and h would be scaled distances and would never become zero unless the antenna was infinite in length.

Therefore, the problem could be solved by rebuilding the array such that the distance between cavities was scaled correctly. However, before

rebuilding the entire array in this fashion, it was thought wise to verify that the original feedline design was correct for the cavities with resonant frequencies below 4.2 GHz. A feed network was then constructed, as described earlier, to excite only the 11 largest elements of the array. Figure 22 shows the resultant feedline. The most severe drawback of this decision was that the electrical bandwidth would be much smaller than originally planned. However, if the antenna would work in the 11 cavity configuration, the bandwidth, theoretically, could be extended by rebuilding the array such that the distances between cavities was scaled correctly.

As with the prototypes, the coupling apertures were cut in the other side of the feed network. Finally, the antenna bottom/feed network was attached to the array with brass screws tapped into the 1/8" brass.

5.2 S Parameter Measurement

To make S parameter measurements of the array, the same sequence as was used for measurement of the prototypes was followed with a few exceptions. First, the frequency range of the 11 cavity array was broader (1.0 - 4.5 GHz). Second, the measurement plane for the array was set at Port 2 of the antenna array (see Figure 22).

The results of these measurements appear in Figures 23-24. The S_{11} locus of Figure 23 behaves as expected for a log-periodic array of cavity-backed slots, as did the S_{21} locus of Figure 23. Note from Figure 23 that the antenna is moderately well matched. In fact, comparison with Szmurlo's S_{11} locus (Figure 25) indicates that the 11 cavity array is matched much better than previous CBS arrays. To improve the impedance

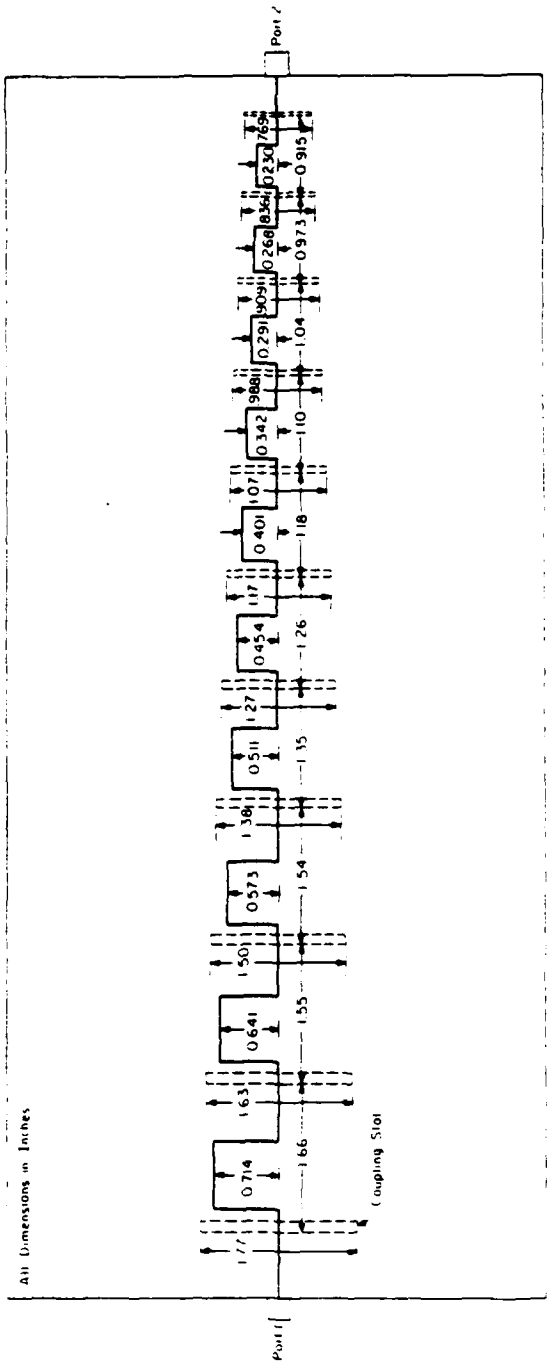

Figure 22. Eleven cavity array feedline.

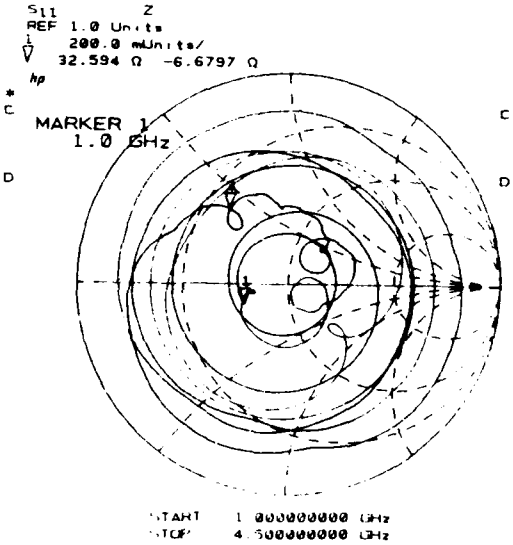

Figure 23.
Measured S_{11} - 11 cavity array.

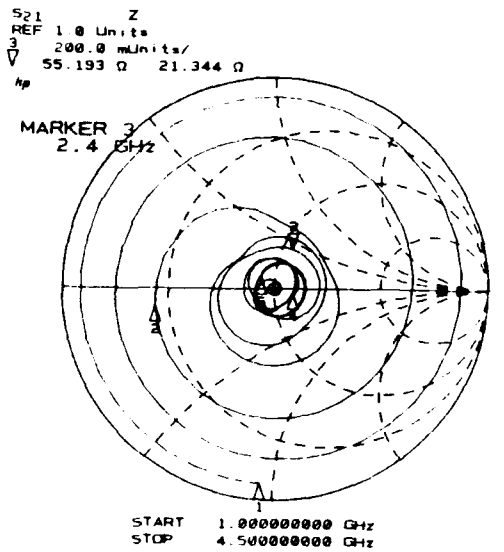

Figure 24.
Measured S_{21} - 11 cavity array.

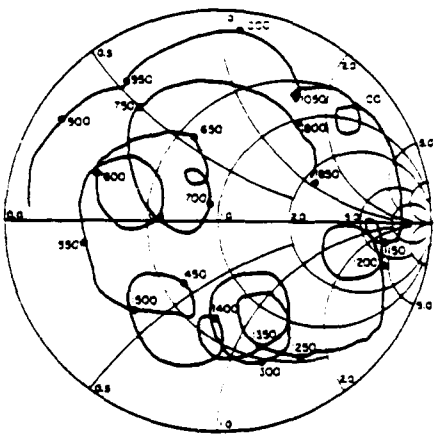

Figure 25.
S_{11} - Szmurlo's 6 cavity array with unmodulated feed.
(Frequencies in MHz)

match of his antenna, Szmurlo modulated the impedance of his feed network to eliminate the structural stopband. This technique of feedline modulation was first described by Ingerson and Mayes and has been successful in improving LP antenna performance. The application of their technique to this research is discussed in Chapter 6.

5.3 Antenna Array Pattern Measurements

Antenna pattern measurements were made at the 20 × 20 foot University of Illinois Electromagnetics Laboratory Ground Plane Range. For the azimuthal patterns, the 11 cavity array was rotated and acted as the transmitting antenna, and a log-periodic array of half trapezoids over a ground plane was used as the receiving antenna. For elevation measurements, the 11 cavity array was the transmitting antenna, and a dipole mounted in a corner reflector (or horn antenna) attached to a fiberglass boom was used as the receiving antenna. The results of these measurements are shown in Figures 26 and 27.

These antenna patterns were measured strictly to verify the antenna had backfire radiation and that the pattern shape was essentially the same over a fairly broad frequency bandwidth. The measurements show good backfire radiation, and the shape of the patterns are alike over the range 1.75 GHz to 3.5 GHz. It is also evident that the patterns do not have an infinite front-to-back ratio. This, however, was expected because the antenna feed network was not designed to cause an infinite front-to-back ratio, but to cause backfire radiation (see Section 5.1).

Patterns were also made in the University of Illinois Electromagnetics Laboratory Anechoic Chamber to determine if a large percentage of energy was being radiated through the coupling apertures. The antenna array was set up with the slots perpendicular to the floor and rotated through 360°. The patterns (Appendix E) display the radiation through the radiating slots in the 0 - 180° range, and the radiation through the

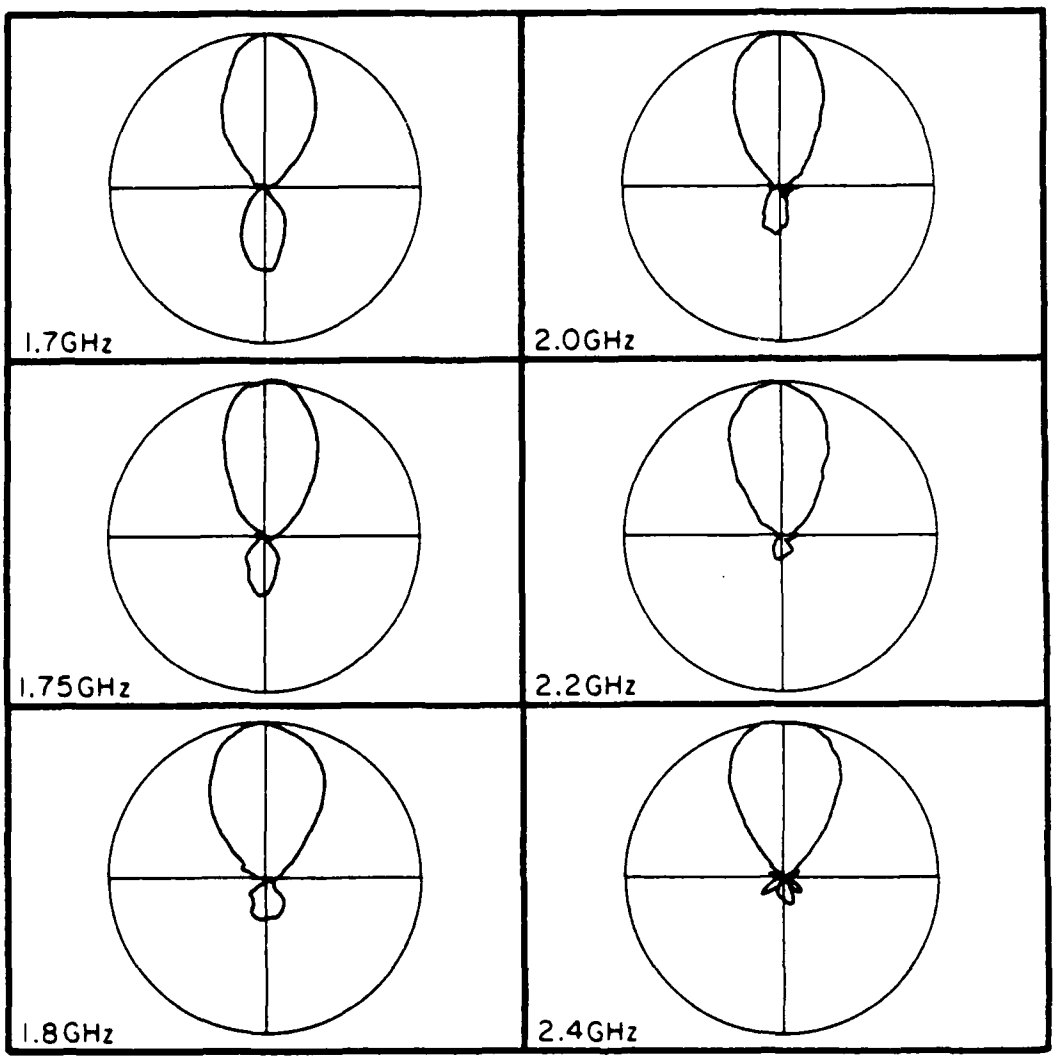

Figure 26.

Azimuthal patterns for 11 cavity array.

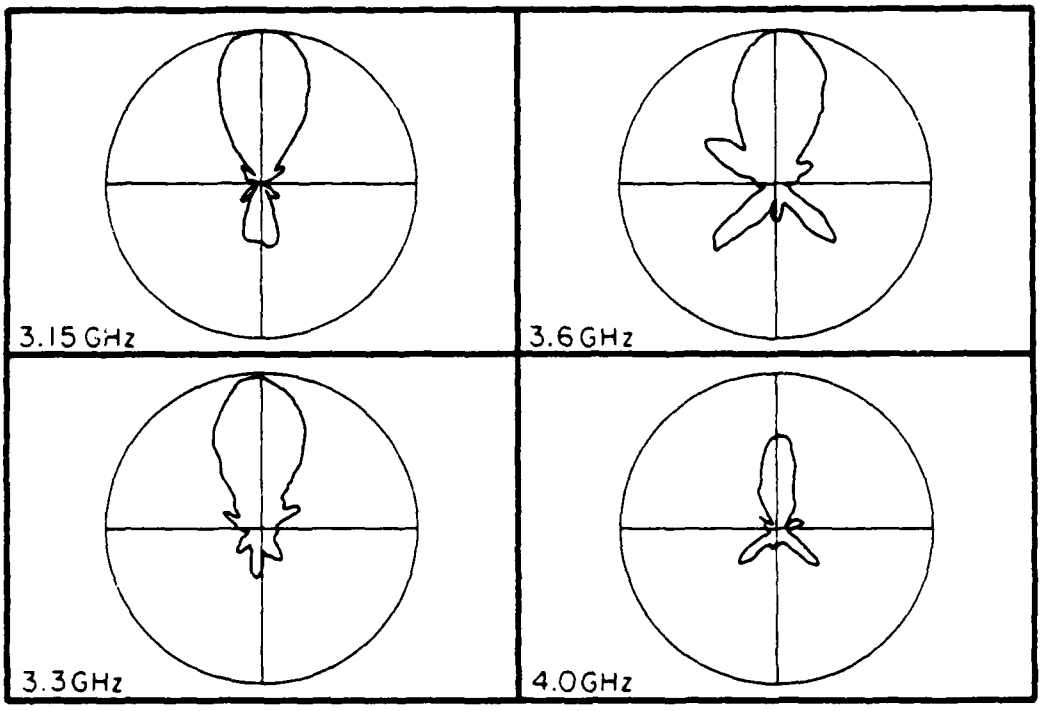

Figure 26. (continued).

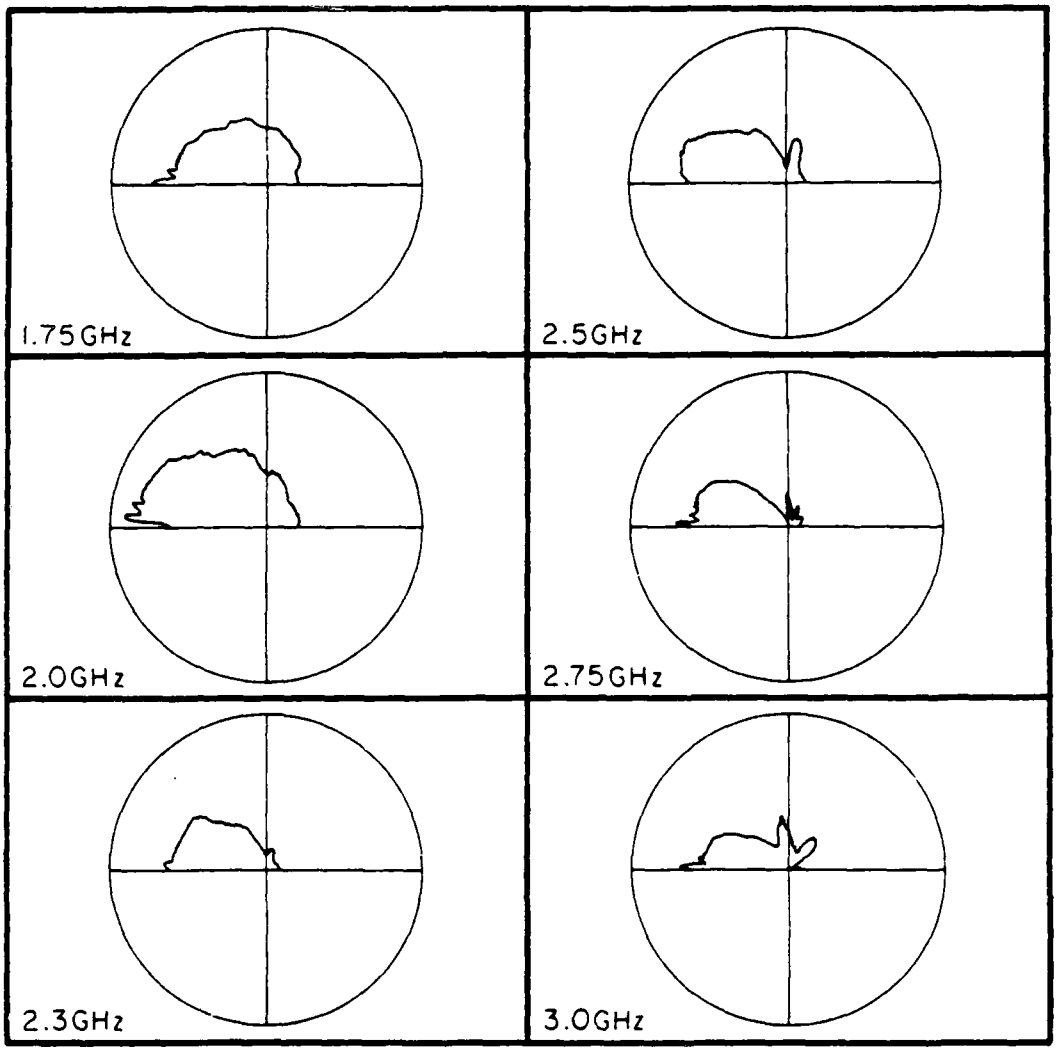

Figure 27.

Elevation patterns for 11 cavity array.

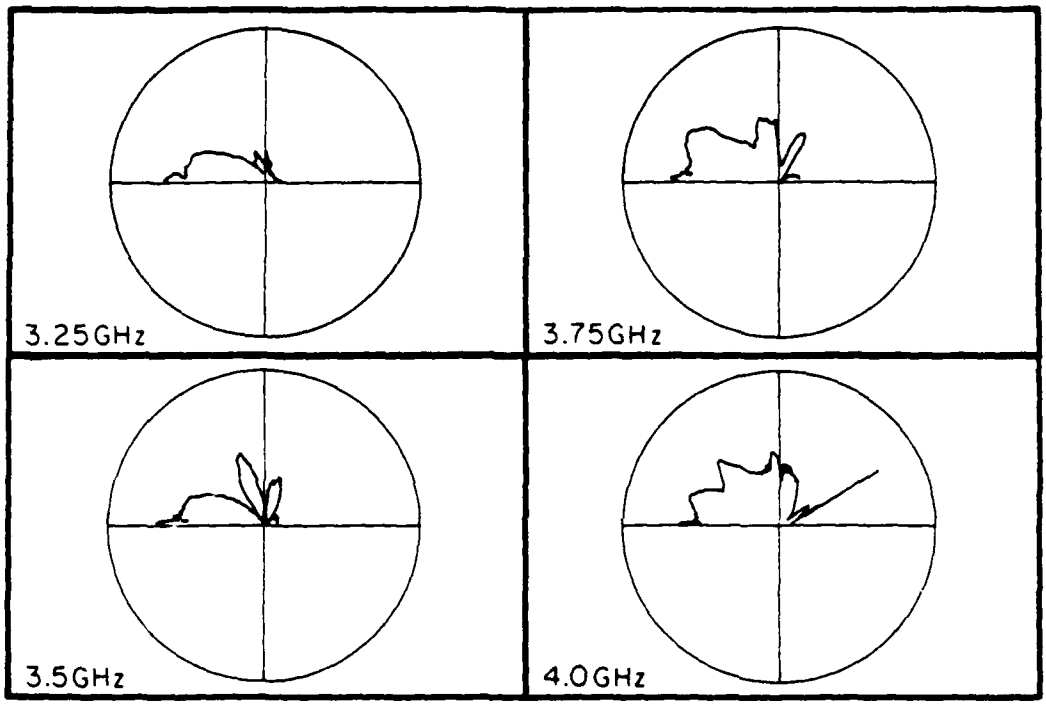

Figure 27. (continued).

coupling slots in the 180° - 360° range. In all cases, the patterns corresponding to radiation through the coupling slots are at least 10 dB below the patterns corresponding to radiation through the radiating slots.

CHAPTER 6
COMPUTER SIMULATION AND STOPBAND ANALYSIS

Although the impedance match of the 11 cavity array was an improvement over those for previous LPCBS arrays, it was expected that it could be improved still more by elimination of the structural stopband through modulation of the feed network impedance. The computer was employed as an aid in locating the structural stopband and in determining what the impedance of the modulated sections of the feedline should be to eliminate the structural stopband. Finally, a computer program modeling the 11 cavity array was run first without and then with the modulated sections of line included to determine if the impedance match was improved. A description of the model used and the results of these computer analyses are presented in this chapter.

6.1 The Shorted-Stub Model of a Single Cavity

The shorted-stub model of a single cavity has been shown to be adequate for use in modeling LPCBS arrays [5]. The model shown in Figure 28 consists of three parameters: the shunt conductance GS(m), the stub characteristic admittance GOS(m), and the stub length (m). The first step

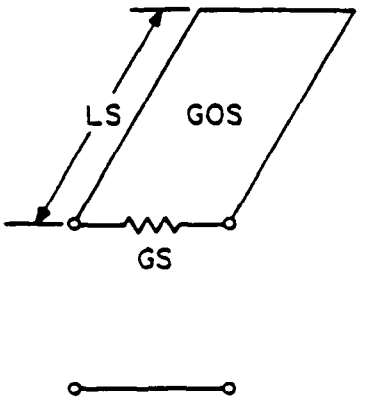

Figure 28. Shorted-stub model of cavity [5].

in effectively modeling the 11 cavity array was to determine the values of GS, GOS and LS which yielded an S_{11} locus for the cavity model that was similar to the S_{11} locus for Prototype 1. It is especially important that the value of S_{11} at resonance is the same for both the model and the prototype.

At resonance (1.78 GHz), the return loss of Prototype 1 was 8.8828 dB. Thus, $|S_{11}|$ at resonance equals 0.35963. The values of LS and GS necessary for the model to yield $|S_{11}| = 0.35963$ at 1.78 GHz can be realized analytically through use of general network parameter (A, B, C, D or chain matrix) analysis. The final parameter, GOS, can be realized by trial and error through use of a computer program such as the one in Appendix A. The resultant values for the model parameters are LS = 0.042135 m, GS = 17.806 m℧, and GOS = 831 m℧. Figure 29a shows the S_{11} locus from the model with these values of LS, GS, GOS, while Figure 29b shows the actual S_{11} locus of Prototype 1.

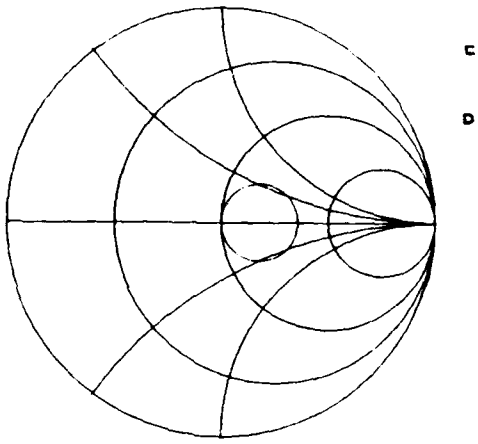

Figure 29a.

Computed S_{11} using cavity model.

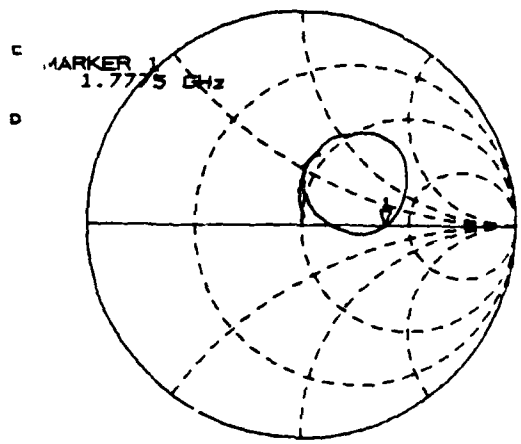

Figure 29b.

Measured S_{11} - Prototype 1. (0.75 - 2.25 GHz)

It is evident that the agreement between the model and Prototype 1 is good, particularly around resonance (1.78 GHz).

The next step was to surround the cavity model with sections of modulated and unmodulated transmission lines to simulate a single cavity fed by a modulated microstrip transmission line. This model is shown in Figure 30.

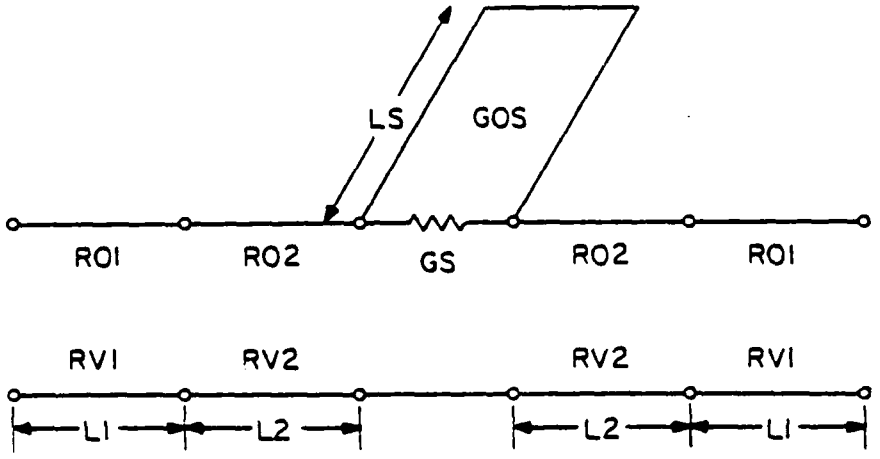

Figure 30. Model of cavity being fed by a modulated microstrip feed [5].

This model now includes all the components of a single element of the array, and is called a cell. With GS = 17.806 mΩ, LS = 0.042135 m, GOS = 831 mΩ, R01 = 50 Ω, L_1 = 0.078, and R02 = 50 Ω, this cell would model the largest element of the 11 cavity array without a modulated feed network. To include the effect of modulation in this cell, L_2 and R02 would be set to the appropriate values for the modulated section of line feeding the largest element. Cells that model smaller array elements can be derived by substituting the correct values (for the element of interest) of L1, L2, R01, R02 and LS for those above. The values of GS, GOS and R0 will be constant for all cells, while the value of LS for cell number n (where n

is defined in Figure 11) will be $(0.042135)(0.92)^{n-2}$. To model the entire array, the cells modeling the individual elements are cascaded (connected end-to-end) in the same order as the elements they model.

6.2 Location of the Structural Stopband

If the cascade of cells described above is approximated as an infinite cascade of identical, symmetrical two ports, image parameter theory can be used to analyze it [5]. To calculate the image parameters of a single cell (or the entire cascade), an A, B, C, D matrix for each component of each cell is formed. These matrices are then multiplied together (in the same order as they occur in the cell/cascade) to yield a resultant A, B, C, D matrix. The image parameters, Z_i = image impedance and γ_i = propagation factor, can then be computed using the elements of the resultant A, B, C, D matrix as follows.

$$Z_i = \sqrt{B/C}$$

$$\gamma_i = \ell n \left(A + \sqrt{A^2 - 1}\right) \quad [5]$$

It is possible to determine the stopband location using either of these parameters. A dramatic change in the magnitude of the image impedance or a phase shift in the imaginary part of the propagation factor indicates the location of the stopband.

A computer program, STPMOD (Appendix B), was written to compute the image parameters in the manner just described for a single unmodulated cell (element number 7, f_r = 3.19 GHz) of the 11 cavity array. The program calculated the image parameters at discrete frequencies from 2-4 GHz. The location of the stopband could then be determined from an examination of

the data. Once the location of the structural stopband for element number 7 was known, the location of the structural stopband for any element could be found by scaling the stopband range of element number 7.

The output of STPMOD for element number 7 is shown graphically in Figures 31 and 32. The first of these figures displays $|Z_i|$ as a function

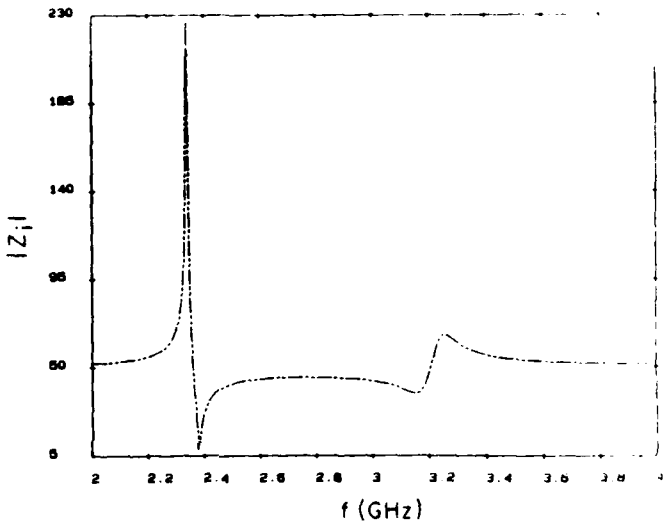

Figure 31. $|Z_i|$ versus f(GHz) - Element 7 with unmodulated feedline.

of frequency. It is immediately obvious from looking at this figure that there is a dramatic change in $|Z_i|$ over the range 2.35 to 2.38 GHz. This is the location of the structural stopband. In this region, the image impedance is far greater in magnitude than the 50 Ω impedance of the feedline. Because of the severe mismatch in this stopband, reflections add up in this region and prevent the incident wave from propagating farther down the feedline. Note also that there is a much less dramatic variation in $|Z_i|$ near 3.19 GHz. This is known as the two-terminal stopband [2] and

normally occurs, as it does in this case, at the resonant frequency of the stub. As evidenced by the small variation in $|Z_i|$ in this region, the impact of the two-terminal stopband is much less than that of the structural stopband.

Figure 32 is a graphical display of the variation of the phase with frequency. Again, the location of the structural stopband can be

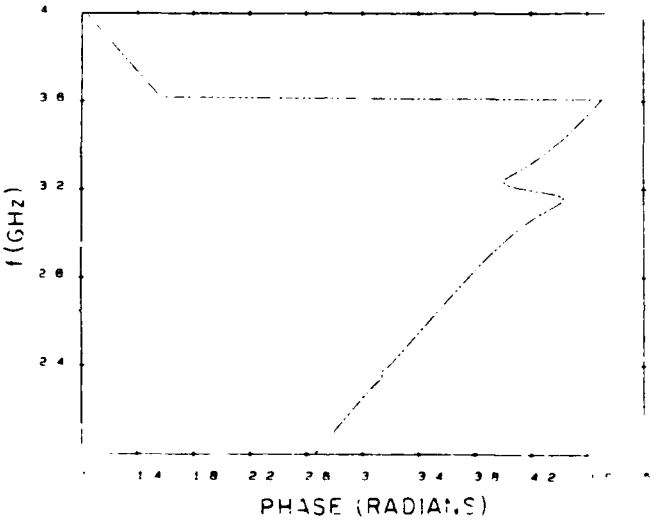

Figure 32. Phase versus f (GHz) - Element 7 with unmodulated feedline.

pinpointed from this figure. Note that in the structural stopband region (from 2.35 to 2.38 GHz), the value of β_i remains constant at π. The two-terminal stopband and the high frequency stopband are also evident. Of special interest in this figure (and the last) is the width of the structural stopband: 0.04 GHz. In comparison to previous LPCBS arrays, this number is very small. Szmurlo, for example, encountered structural

stopbands as great as 0.15 GHz in width as seen from Figure 33 [5]. Furthermore, the structural stopband encountered in this research is about

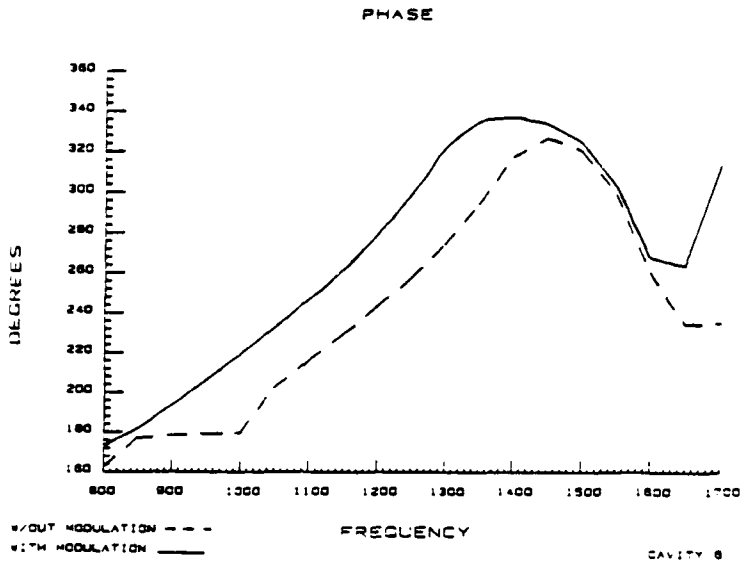

Figure 33. Phase versus f (MHz) - Szmurlo's cavity 6.

2% of the projected operating bandwidth of the 11 cavity array, as compared with about 43% for Szmurlo's antenna (for an operating bandwidth of 975 to 1325 MHz). The impact of the narrow structural stopband is discussed in detail in Section 6.5.

6.3 Eliminating the Structural Stopband

If the image impedance in the stopband region is made to be 50 ohms, the structural stopband will effectively be matched out. As mentioned before, modulation of the feedline impedance has historically minimized the impact of the structural stopband. The difficulty was to determine the length and impedance of the modulated sections of the line (L2 and R02). As it turned out, the length of the modulated section was more or less

fixed by physical constraints of the feed network; thus, only R02 had to be found to complete the design of the modulated cell.

For this task, another computer program, ITMOD (Appendix C), was created. The required inputs for ITMOD are the center frequency of the structural stopband and a range of possible modulation impedances. The output of the program is $|Z_i|$ (at the stopband center frequency) as a function of possible modulation impedances. After numerous executions of this program, it was discovered that the modulation impedance which yielded a value for $|Z_i|$ closest to 50 ohms was R02 = 47.3245976 Ω. This was a startling result because, compared to the modulation impedances of previous LPCBS arrays (e.g., modulation impedance for Szmurlo's antenna < 30 Ω), it is surprisingly close to 50 Ω.

To verify that the correct modulation impedance had indeed been found, STPMOD was run again with R02 = 47.3245976 and L1 and L2 adjusted for inclusion of the modulated section in the cell. The results (Figures 34 and 35) show that the structural stopband impact had indeed been greatly decreased because of the modulated feedline. In fact, the structural stopband is not visible in Figure 35. In other words, the data verified that R02 = 47.3245976 was, in fact, correct.

6.4 Effect of Eliminating the Structural Stopband on Antenna Impedance

Before making any modifications to the antenna, it was considered wise to check, through the use of a computer program, the effect of modulation on the antenna impedance. Hence, a program using chain matrix multiplication as described in Section 6.2 was written to calculate S_{11} for the 11 cavity

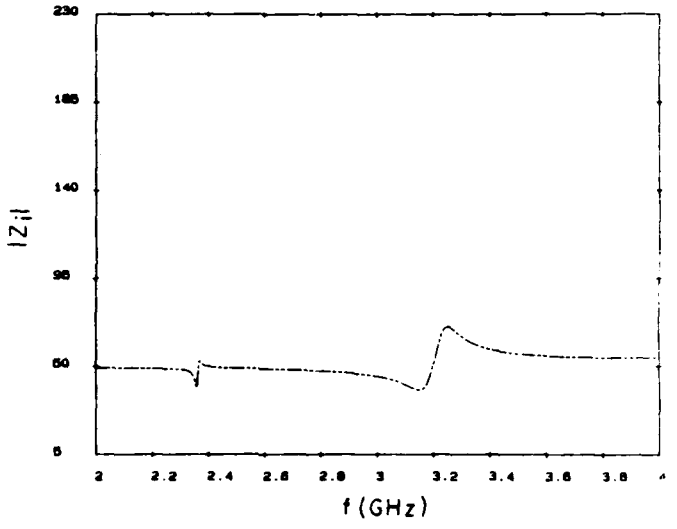

Figure 34.

$|Z_i|$ versus f (GHz) - Element 7 with modulated feedline.

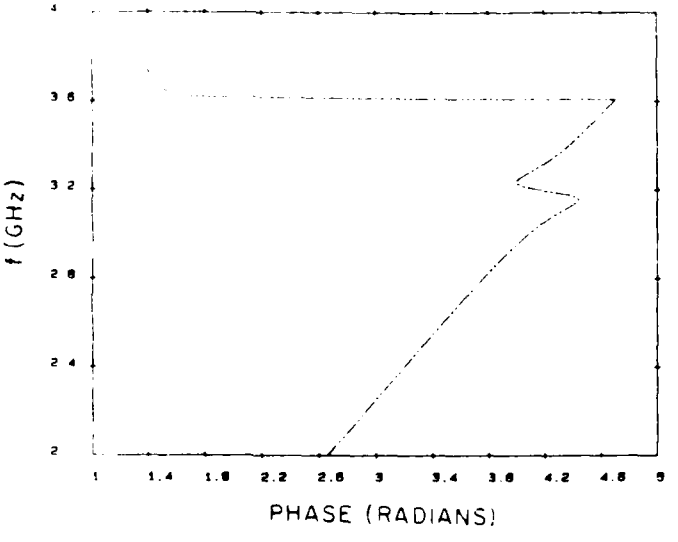

Figure 35.

Phase versus f (GHz) - Element 7 with modulated feedline.

array. The program, MODANT (Appendix D), was first run for the case of the antenna without modulation, i.e., the impedance of all modulated sections was set to 50 Ω. The computed S_{11} locus using MODANT for the 11 cavity model over the frequency range from 1.0 to 4.5 GHz is displayed in Figure 36. Although there is not point-to-point agreement between Figure 36

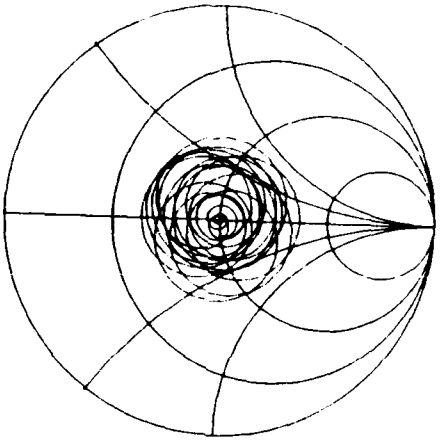

Figure 36. Computed S_{11} - 11 cavity array with unmodulated feedline. (1.0 to 4.5 GHz)

and the measured S_{11} for the 11 cavity array (Figure 23), the general shape and position of the two loci on the Smith Chart indicate that the 11 cavity model is an adequate representation of the actual antenna.

Next, the program was run again; this time, however, the modulated sections of line were included. The S_{11} locus for this case is shown in Figure 37. There is very little difference between Figures 36 and 37.

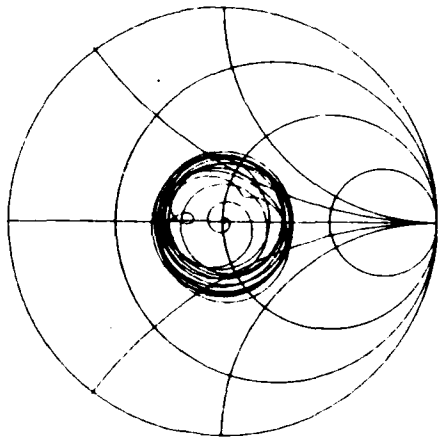

Figure 37. Computed S_{11} - 11 cavity array with modulated feedline. (1.0 to 4.5 GHz)

The major difference is that the locus in the latter figure does not move in toward the center of the chart as the locus of the first figure does. However, the impedance match (as indicated by the distance from the center of the chart to the locus) has not improved with modulation.

6.5 Cause and Impact of the Narrow Stopband

The probable reason for the slight impact of modulating the feedline is that the stopband seems to have little effect on the antenna impedance for this array. Therefore eliminating it through modulation yields little improvement. The evidence for this assumption includes the fact that the

impedance of the unmodulated antenna is rather good in comparison to those for previous LPCBS arrays, the stopband for the antenna is very narrow both in relation to the projected bandwidth and to the stopband of previous LPCBS arrays, and the modulation impedance to eliminate the stopband is very close to 50 ohms. In fact, the modulation impedance is so close to 50 Ω that the modulated section of the microstrip line would be virtually the same width as the unmodulated section.

These factors indicated that the structural stopband was not significantly degrading antenna performance. Therefore, it was decided that modulation of the feedline would not improve the antenna performance and would, therefore, be unnecessary. This development is both startling and exciting because it greatly simplifies feedline design. Not only will the construction of feedlines be easier, but the computer simulation to determine the modulation impedance will now be unnecessary. Certainly, this development should be exploited fully. Therefore, it is very important to understand what caused the structural stopband to be so narrow and to have such little impact on antenna performance.

Recall from Chapter 3 that Prototype 1 (with a coupling slot length of 4.5 cm) was a much better matched antenna than previous CBS elements. Clearly, if the individual elements of an LP array are well matched, the array itself will have a better chance of being well matched than if the individual elements are poorly matched. Therefore, the stopband for an antenna with well-matched radiators would have much less effect on antenna performance than the stopband of an antenna with poorly-matched radiators. Why, then, are the elements of this array better matched than previous

LPCBS elements? Again, recall from Chapter 3 that the resonant frequency and impedance at resonance were found to be functions of the length of the coupling slot. In other words, the use of aperture coupling resulted in the ability to create (by varying the coupling slot length) relatively well-matched elements which, in turn, made up a fairly well-matched array. It was concluded that the width and impact of the structural stopband were greatly lessened because of the use of aperture coupling to feed the array elements.

CHAPTER 7
CONCLUSIONS AND RECOMMENDATIONS

The goals for this research were met. The LP array of Aperture-Coupled CBS (LPACCBS) antennas demonstrated the potential for a larger operating bandwidth using less 'real estate' than previous LPCBS antennas. It operated at much higher frequencies than any previous LPCBS array. Moreover, the theory that cavity depths do not have to be faithfully scaled for good frequency independent performance was again validated. In addition, it was discovered that the LPACCBS array was not hindered by the presence of a large structural stopband. This was, perhaps, the most important result of the research.

The goals just enumerated were reached primarily because the LPACCBS antenna introduced two major departures from previous LPCBS design: 'half-width' cavities, and aperture coupling. The use of half-width cavities as suggested by Tanner made it possible for an array of CBS elements to be constructed in about half the space required for previous CBS arrays. Certainly this result will make the CBS array even more attractive to potential users, especially those who have a requirement for conformal mounting in limited space, e.g., aircraft and missile designers.

This research also demonstrated the many clear advantages of using aperture coupling to feed an array of CBS elements. Not only does it eliminate scattering from the feedline, but also offers a new degree of freedom for controlling antenna performance. One demonstrated advantage of this new degree of freedom was the ability to improve the performance of an individual element to such a degree that the antenna array structural stopband is almost nonexistent.

What should be the future research in CBS arrays? Obviously, the advantages of aperture coupling as a feed system for CBS antennas should be closely scrutinized in order to fully exploit this useful tool. In particular, research should be done to utilize aperture coupling as a method to reduce antenna impedance still further by building on this and previous research. One technique that had been successful [3] in reducing antenna impedance in previous CBS antennas was to move the feedline away from the center of the feed slot to a position that resulted in better overall antenna impedance. Unfortunately, since the feed slot and the radiating slot were one and the same, this technique resulted in asymmetrical patterns and had to be abandoned. Because aperture coupling does not combine the feed (coupling) slot and the radiating slot, this scattering will not occur. Thus, patterns will not be affected by an effort to improve impedance through lateral shifting of the feedline below the coupling slot. Ultimately, perhaps the impedance match between the array elements and the feedline could be improved enough through aperture coupling to eliminate the structural stopband completely. In any case, the application of aperture coupling to CBS arrays, based on this research alone, looks extremely promising and certainly merits more attention.

APPENDIX A

COMPUTER PROGRAM TO CALCULATE S PARAMETERS OF SHORTED STUB MODEL

```
      PROGRAM SPARM(INPUT,OUTPUT)
C
C     MODIFIED PROGRAM FROM APPENDIX A OF SZMURLO [5]
C     PROGRAM CALCULATED S PARAMETERS FOR GIVEN VARIABLES IN
C     SHORTED STUB MODEL
C
      REAL LS
      COMPLEX A,B,C,D,DEN,Y,S11,S12
C
      OPEN  (UNIT=6,FILE='SOUT',STATUS='NEW')
C
      PRINT *,'ENTER CHAR. ADMITT. OF STUB IN MILLIMHOS'
      READ *,GOS
      WRITE (6,*) 'CHAR. ADMITT. OF STUB IN MILLIMHOS ',GOS
C
      PRINT *,'ENTER SHUNT CONDUCTANCE IN MILLIMHOS'
      READ *,GS
      WRITE (6,*) 'SHUNT COND. MILLIMHOS',GS
C
      PRINT*,'ENTER CHAR. IMPEDANCE OF MAIN LINE IN OHMS'
      READ *,RO
      WRITE (6,*) 'MAIN LINE CHAR. IMP. ',RO
C
      PRINT*,'ENTER LENGTH OF STUB IN CENTIMETERS'
      READ *,LS
      WRITE (6,*) 'LENGTH OF STUB (CM) ',LS
C
      PRINT*,'ENTER LOWER FREQUENCY LIMIT IN GHZ'
      READ *,FL
      WRITE (6,*) 'LOWER FREQ. ',FL
C
      PRINT*,'ENTER UPPER FREQUENCY LIMIT IN GHZ'
      READ *,FU
      WRITE (6,*) 'UPPER FREQ. ',FU
C
      PRINT*,'ENTER FREQUENCY INCREMENT IN GHZ'
      READ *,DF
      WRITE (6,*) 'DELTA FREQ. ',DF
C
      PI=4.*ATAN(1.)
      TOPI=2.*PI
C
      GO=1./RO
      N=0
C
      WRITE(6,*) '  '
      WRITE(6,*) '  '
      WRITE (6,*)'FREQ S11 R/I S12 R/I S11 M/A S12 M/A'
C
C
   30 F=FL+N*DF
      WVLN=30./F
      ALOLAM=LS/WVLN
      THETS=TOPI*ALOLAM
C
      BSTUB=-(GOS*1.E-3)/TAN(THETS)
      Y=CMPLX(GS*1.E-3,BSTUB)
      B=1./Y
      A=(1.,0.)
      C=(0.,0.)
      D=(1.,0.)
      DEN=2.*B*GO
C
      S11=(B*GO)/DEN
      S12=2./DEN
C
```

```
      S11M=CABS(S11)
      S11A=(360./TOPI)*ATAN2(AIMAG(S11),REAL(S11))
C
      S12M=CABS(S12)
      S12A=(360./TOPI)*ATAN2(AIMAG(S12),REAL(S12))
C
      WRITE (6,*) F,S11,S12,S11M,S11A,S12M,S12A
      N=N+1
      IF (F-FU) 30,30,40
C
   40 CONTINUE
      STOP
      END
```

APPENDIX B

COMPUTER PROGRAM TO LOCATE THE STRUCTURAL STOPBAND

```
      PROGRAM STPMOD
C
C     PROGRAM TO LOCATE THE STRUCTURAL STOPBAND
C
      COMPLEX J(2,2),A(2,2),B(2,2),C(2,2),ZI,GAM,D(2,2),E(2,2),G(2,2)
      REAL F,LS,GS,GOS,LAMDA,BETA,LL,PI,RM,YM,TWOPI,MAGZ,W,AA,AREAL
      REAL X,YMOD,LM,BB
      CHARACTER*8 DATA1,DATA2,DATA3,DATA4
C
      COMMON/VARS1/J,LL,PHASEDE
      COMMON/VARS2/A
      COMMON/VARS3/D,FASEDE,YMOD
C
      DATA ENDIT/-1.234/
C
   10 FORMAT(1X,'FREQ',10X,'/A/',15X,'ZI',10X,'/ZI/',11X,'GAMMA')
   11 FORMAT(F7.5,F18.14,6F9.3)
C
      OPEN(UNIT=6,FILE='IT',STATUS='NEW')
C
      WRITE(*,*)' '
      WRITE(*,*)'FILENAME FOR PHASE DATA'
      READ*, DATA1
      WRITE(*,*)'FILENAME FOR ATTENUATION DATA'
      READ*, DATA2
      WRITE(*,*)'FILENAME FOR /A/ DATA'
      READ*,DATA3
      WRITE(*,*)'FILENAME FOR /ZI/ DATA'
      READ*,DATA4
      OPEN(UNIT=14,FILE=DATA1)
      OPEN(UNIT=15,FILE=DATA2)
      OPEN(UNIT=16,FILE=DATA3)
      OPEN(UNIT=17,FILE=DATA4)
C
C
C     INPUT THE MODULATION IMPEDANCE
C
      X=50.
C
      WRITE(6,*)' '
      WRITE(6,*)' '
      WRITE(6,*)'MODULATION IMPEDANCE =',X,' OHMS'
      WRITE(6,*)' '
      WRITE(6,10)
      WRITE(6,*)' '
C
C     INITIALIZE OTHER VARIABLES
C
      PI=4.*ATAN(1.)
      TWOPI=2.*PI
C
      DO 100 W=2,4,.01
C
      F=W*1.E9
      LS=.042135*(.92**7)
      GS=17.806
      GOS=631.
      LAMDA=3.E8/F
      BETA=TWOPI/LAMDA
      RM=47.387135
      YM=1./RM
      YMOD=1./X
C
C
C     INTRODUCE LINE LENGTH OF UNMODULATED SECTIONS
C
```

```
      LL=.0215-(.003)/(.92**3)
C
C     INTRODUCE LINE LENGTH OF MODULATED SECTIONS
      LM=(.003)/(.92**3)
C
C     CREATE THE FIRST UNMODULATED LINE MATRIX
C
      CALL LMAT(BETA,RM,YM)
C
C
C     CREATE THE FIRST MODULATED LINE MATRIX
C
      CALL MMAT (BETA,LM,X)
C
C     MULTIPLY THE FIRST TWO MATRICES TOGETHER
C
      CALL MATMUL(E,J,D)
C
C     CREATE THE FIRST CAVITY MATRIX
C
      CALL CMAT(BETA,LS,GOS,GS)
C
C     MULTIPLY END MATRIX ON RIGHT BY CAVITY MATRIX
C
      CALL MATMUL(B,E,A)
C
C     MULTIPLY END MATRIX ON RIGHT BY MODULATED LINE MATRIX
C
      CALL MATMUL(G,B,D)
C
C     MULTIPLY END MATRIX ON RIGHT BY UNMODULATED LINE MATRIX
C
      CALL MATMUL(C,G,J)
C
      ZI=CSQRT(C(1,2)/C(2,1))
      MAGZ=CABS(ZI)
      AA=CABS(C(1,1))
C
      GAM=CLOG(C(1,1)+CSQRT(C(1,1)**2-1.))
      BB=AIMAG(GAM)
      IF(BB.LT.0.)BB=BB+TWOPI
      BB=TWOPI-BB
      WRITE(6,11)W,AA,ZI,MAGZ,GAM
      WRITE(14,555)BB,',  ',W
      WRITE(15,555)REAL(GAM),',  ',W
      WRITE(16,556)AA,',  ',W
      WRITE(17,557)W,',  ',MAGZ
C
  100 CONTINUE
  555 FORMAT(F8.5,A3,F8.5)
  556 FORMAT(F17.14,A3,F8.5)
  557 FORMAT(F8.5,A3,F10.5)
  558 FORMAT(F7.3,A3,F7.3)
      WRITE(14,558)ENDIT,',  ',ENDIT
      WRITE(15,558)ENDIT,',  ',ENDIT
      WRITE(16,558)ENDIT,',  ',ENDIT
      WRITE(17,558)ENDIT,',  ',ENDIT
      END
C
      SUBROUTINE LMAT(BETA,RM,YM)
C
      COMPLEX J(2,2)
      REAL BETA,LL,RM,YM
C
      COMMON/VARS1/J,LL,PHASEDE
      PHASEDE=BETA*LL*(2.146**.5)
```

```
      J(1,1)=CMPLX(COS(PHASEDE),0.)
      J(1,2)=CMPLX(0.,RM*SIN(PHASEDE))
      J(2,1)=CMPLX(0.,YM*SIN(PHASEDE))
      J(2,2)=CMPLX(COS(PHASEDE),0.)
      RETURN
      END
C
C
      SUBROUTINE MMAT(BETA,LM,X)
C
      COMPLEX D(2,2)
      REAL BETA,LM,X,YMOD
C
      COMMON/VARS3/D,FASEDE,YMOD
      FASEDE=BETA*LM*(2.146**.5)
      D(1,1)=CMPLX(COS(FASEDE),0.)
      D(1,2)=CMPLX(0.,X*SIN(FASEDE))
      D(2,1)=CMPLX(0.,YMOD*SIN(FASEDE))
      D(2,2)=CMPLX(COS(FASEDE),0.)
      RETURN
      END
C
C
      SUBROUTINE CMAT(BETA,LS,GOS,GS)
C
      COMPLEX A(2,2),YCAV
      REAL LS,BETA,GOS,GS
C
      COMMON/VARS2/A
C
      BETADE=BETA*LS
      BSTUB=-(GOS*1.E-3)/TAN(BETADE)
      YCAV=CMPLX(GS*1.E-3,BSTUB)
      A(1,1)=CMPLX(1.,0.)
      A(1,2)=1./YCAV
      A(2,1)=CMPLX(0.,0.)
      A(2,2)=CMPLX(1.,0.)
      LS=LS*0.92
      RETURN
      END
C
C
      SUBROUTINE MATMUL(X,Y,Z)
C
C     SUBROUTINE RETURNS X=YZ
C
      COMPLEX X(2,2),Y(2,2),Z(2,2)
C
      X(1,1)=Y(1,1)*Z(1,1)+Y(1,2)*Z(2,1)
      X(1,2)=Y(1,1)*Z(1,2)+Y(1,2)*Z(2,2)
      X(2,1)=Y(2,1)*Z(1,1)+Y(2,2)*Z(2,1)
      X(2,2)=Y(2,1)*Z(1,2)+Y(2,2)*Z(2,2)
      RETURN
      END
```

APPENDIX C

COMPUTER PROGRAM TO DETERMINE THE IMPEDANCE OF THE MODULATED LINE

```
      PROGRAM ITMOD
C
C     PROGRAM TO DETERMINE THE IMPEDANCE OF THE MODULATED LINE
C
      COMPLEX J(2,2),A(2,2),B(2,2),C(2,2),ZI,GAM,D(2,2),E(2,2),G(2,2)
      REAL F,LS,GS,GOS,LAMDA,BETA,LL,PI,RM,YM,TWOPI,MAGZ,W,AA,AREAL
      REAL X,YMOD,LM
C
      COMMON/VARS1/J,LL,PHASEDE
      COMMON/VARS2/A
      COMMON/VARS3/D,FASEDE,YMOD
C
   10 FORMAT('RMOD',7X,'/A/',9X,'/ZI/',15X,'GAMMA')
   11 FORMAT(F6.3,6F9.7)
C
      OPEN(UNIT=6,FILE='IT',STATUS='NEW')
C
      WRITE(6,*)' '
      WRITE(6,*)' '
      WRITE(6,10)
      WRITE(6,*)' '
C
C     INITIALIZE VARIABLES
C
      PI=4.*ATAN(1.)
      TWOPI=2.*PI
C
      DO 100 X=47.32459,47.3246,.0000001
C
      F=2.3608*1.E9
      LS=.042135*(.92**7)
      GS=17.806
      GOS=831.
      LAMDA=3.E8/F
      BETA=TWOPI/LAMDA
      RM=50.
      YM=1./RM
      YMOD=1./X
C
C
C     INTRODUCE LINE LENGTH OF UNMODULATED SECTIONS
C
      LL=.0215-(.003)/(.92**3)
C
C     INTRODUCE LINE LENGTH OF MODULATED SECTIONS
      LM=(.003)/(.92**3)
C
C     CREATE THE FIRST UNMODULATED LINE MATRIX
C
      CALL LMAT(BETA,RM,YM)
C
C
C     CREATE THE FIRST MODULATED LINE MATRIX
C
      CALL MMAT (BETA,LM,X)
C
C     MULTIPLY THE FIRST TWO MATRICES TOGETHER
C
      CALL MATMUL(E,J,D)
C
C     CREATE THE FIRST CAVITY MATRIX
C
      CALL CMAT(BETA,LS,GOS,GS)
C
C     MULTIPLY END MATRIX ON RIGHT BY CAVITY MATRIX
C
```

```
      CALL MATMUL(B,E,A)
C
C     MULTIPLY END MATRIX ON RIGHT BY MODULATED LINE MATRIX
C
      CALL MATMUL(C,B,D)
C
C     MULTIPLY END MATRIX ON RIGHT BY UNMODULATED LINE MATRIX
C
      CALL MATMUL(C,G,J)
C
      ZI=CSQRT(C(1,2)/C(2,1))
      MAGZ=CABS(ZI)
      AA=CABS(C(1,1))
C
      GAM=CLOG(C(1,1)+CSQRT(C(1,1)**2-1.))
      WRITE(6,*)X,AA,MAGZ,GAM
  100 CONTINUE
      END
C
      SUBROUTINE LMAT(BETA,RM,YM)
C
      COMPLEX J(2,2)
      REAL BETA,LL,RM,YM
C
      COMMON/VARS1/J,LL,PHASEDE
      PHASEDE=BETA*LL*(2.1&6**.5)
      J(1,1)=CMPLX(COS(PHASEDE),0.)
      J(1,2)=CMPLX(0.,RM*SIN(PHASEDE))
      J(2,1)=CMPLX(0.,YM*SIN(PHASEDE))
      J(2,2)=CMPLX(COS(PHASEDE),0.)
      RETURN
      END
C
C
      SUBROUTINE MMAT(BETA,LM,X)
C
      COMPLEX D(2,2)
      REAL BETA,LM,X,YMOD
C
      COMMON/VARS3/D,FASEDE,YMOD
      FASEDE=BETA*LM*(2.1&6**.5)
      D(1,1)=CMPLX(COS(FASEDE),0.)
      D(1,2)=CMPLX(0.,X*SIN(FASEDE))
      D(2,1)=CMPLX(0.,YMOD*SIN(FASEDE))
      D(2,2)=CMPLX(COS(FASEDE),0.)
      RETURN
      END
C
C
      SUBROUTINE CMAT(BETA,LS,GOS,GS)
C
      COMPLEX A(2,2),YCAV
      REAL LS,BETA,GOS,GS
C
      COMMON/VARS2/A
C
      BETADE=BETA*LS
      BSTUB=-(GOS*1.E-3)/TAN(BETADE)
      YCAV=CMPLX(GS*1.E-3,BSTUB)
      A(1,1)=CMPLX(1.,0.)
      A(1,2)=1./YCAV
      A(2,1)=CMPLX(0.,0.)
      A(2,2)=CMPLX(1.,0.)
      LS=LS*0.92
      RETURN
      END
```

```
C
C
      SUBROUTINE MATMUL(X,Y,Z)
C
C     SUBROUTINE RETURNS X=YZ
C
      COMPLEX X(2,2),Y(2,2),Z(2,2)
C
      X(1,1)=Y(1,1)*Z(1,1)+Y(1,2)*Z(2,1)
      X(1,2)=Y(1,1)*Z(1,2)+Y(1,2)*Z(2,2)
      X(2,1)=Y(2,1)*Z(1,1)+Y(2,2)*Z(2,1)
      X(2,2)=Y(2,1)*Z(1,2)+Y(2,2)*Z(2,2)
      RETURN
      END
```

APPENDIX D

COMPUTER PROGRAM TO CALCULATE THE S PARAMETERS OF A LPCBS ARRAY

```
      PROGRAM MODANT
C
C     PROGRAM TO CALCULATE THE S-PARAMETERS OF A LPCBS ARRAY
C
      COMPLEX J(2,2),A(2,2),B(2,2),C(2,2),S11,S21,S11IMP,S21IMP,DEN
      COMPLEX D(2,2),E(2,2),G(2,2),H(2,2),NS11IMP,NS21IMP
      REAL F,LS,GS,GOS,LAMDA,BETA,LL(30),LM(30),PI,X(11),YM(11)
      REAL TWOPI,Z0,Y0,ENDIT,S11M
      CHARACTER*8 DATA1,DATA2
C
      COMMON/VARS1/J,LL
      COMMON/VARS2/A
      COMMON/VARS3/D,LM,YM
C
      DATA ENDIT/-1.234/
C
C
   10 FORMAT(2X,'FREQ',9X,'S11',15X,'S21',13X,'NS11IMP.',10X,'NS21IMP.')
   11 FORMAT(F6.3,8F9.3)
C
      OPEN(UNIT=6,FILE='S11S21',STATUS='NEW')
C
      WRITE(*,*) ' '
      WRITE(*,*) 'FILENAME FOR NS11IMP DATA'
      READ*, DATA1
      WRITE(*,*) 'FILENAME FOR NS21IMP DATA'
      READ*, DATA2
      OPEN(UNIT=14,FILE=DATA1)
      OPEN(UNIT=15,FILE=DATA2)
C
      WRITE(6,*)' '
      WRITE(6,*)' '
      WRITE(6,10)
      WRITE(6,*)' '
C
C     INITIALIZE VARIABLES
C
      PI=4.*ATAN(1.)
      TWOPI=2.*PI
C
      DO 100 W=1,4.5,0.005
C
      F=W*1.E9
      LS=.0183030
      GS=17.806
      GOS=831.
      LAMDA=3.E8/F
      BETA=TWOPI/LAMDA
C
      Z0=50.
      Y0=1./Z0
C
C     INTRODUCE LINE LENGTHS BETWEEN CAVITIES
C
      I=1
      M=1
      LL(1)=.054388
      LL(2)=.028675
      LL(3)=.031511
      LL(4)=.034594
      LL(5)=.037948
      LL(6)=.041587
      LL(7)=.045545
      LL(8)=.049848
      LL(9)=.054525
      LL(10)=.059609
```

```
      LL(11)=.065134
      LL(12)=.054982
C
C     INTRODUCE MODULATED LINE LENGTHS
C
      DO 40 K=1,11,1
      LM(K)=.003/(.92**(K-1))
   40 CONTINUE
C
C     INTRODUCE CHARACTERISTIC RESISTANCE OF MODULATED SECTIONS
C
      DO 45 K=1,11,1
      X(K)=47.387135
   45 CONTINUE
C
C     CREATE THE FIRST UNMODULATED LINE MATRIX
C
      CALL LMAT(BETA,I,Z0,Y0)
C
C     CREATE THE FIRST MODULATED LINE MATRIX
C
      CALL MMAT(BETA,M,X)
C
C     MULTIPLY THE FIRST TWO MATRICES TOGETHER
C
      CALL MATMUL(E,J,D)
C
      ISTOP=13
   50 CONTINUE
C
C     CREATE CAVITY MATRIX
C
      CALL CMAT(BETA,LS,GOS,GS)
C
C     MULTIPLY 'END' MATRIX ON RIGHT BY CAVITY MATRIX
C
      CALL MATMUL(B,E,A)
C
C     MULTIPLY 'END' MATRIX ON RIGHT BY MODULATED LINE MATRIX
C
      CALL MATMUL(G,B,D)
C
C     CREATE NEXT UNMODULATED LINE MATRIX
C
      CALL LMAT(BETA,I,Z0,Y0)
C
C     MULTIPLY 'END' MATRIX ON RIGHT BY UNMODULATED LINE MATRIX
C
      CALL MATMUL(C,G,J)
C
      IF(ISTOP-I)60,60,55
   55 CONTINUE
C
C     CREATE NEXT MODULATED LINE MATRIX
C
      CALL MMAT(BETA,M,X)
C
C     MULTIPLY 'END' MATRIX ON RIGHT BY MODULATED LINE MATRIX
C
      CALL MATMUL(E,C,D)
C
      GO TO 50
   60 DEN=(Z0*C(1,1))+C(1,2)+'(Z0**2.)*C(2,1))+(Z0*C(2,2))
      S11=((Z0*C(1,1))+C(1,2)-((Z0**2.)*C(2,1))-(Z0*C(2,2)))/DEN
      S21=(2.*Z0)/DEN
      S11MP=Z1*(1.+S11)/(1.-S11)
```

```
      NS11IMP=S11IMP/Z0
      S21IMP=Z0*(1.+S21)/(1.-S21)
      NS21IMP=S21IMP/Z0
      S11M=CABS(S11)
C
      WRITE(6,11)W,S11,S21,NS11IMP,NS21IMP,S11M
      WRITE(14,555) REAL(NS11IMP),',  ', AIMAG(NS11IMP)
      WRITE(15,555) REAL(NS21IMP),',  ', AIMAG(NS21IMP)
C
C
C
  100 CONTINUE
  555 FORMAT(F10.4,A3,F10.4)
      WRITE(14,555) ENDIT,',  ',ENDIT
      WRITE(15,555) ENDIT,',  ',ENDIT
      END
C
      SUBROUTINE LMAT(BETA,I,Z0,Y0)
C
      COMPLEX J(2,2)
      REAL LL(30)
C
      COMMON/VARS1/J,LL
      PHASEDE=BETA*LL(I)*(2.146**.5)
      J(1,1)=CMPLX(COS(PHASEDE),0.)
      J(1,2)=CMPLX(0.,Z0*SIN(PHASEDE))
      J(2,1)=CMPLX(0.,Y0*SIN(PHASEDE))
      J(2,2)=CMPLX(COS(PHASEDE),0.)
      I=I+1
      RETURN
      END
C
C
      SUBROUTINE MMAT(BETA,M,X)
C
      COMPLEX D(2,2)
      REAL LM(30),X(11),YM(11)
C
      COMMON/VARS3/D,LM,YM
      FASEDE=BETA*LM(M)*(2.146**.5)
      YM(M)=1./X(M)
      D(1,1)=CMPLX(COS(FASEDE),0.)
      D(1,2)=CMPLX(0.,X(M)*SIN(FASEDE))
      D(2,1)=CMPLX(0.,YM(M)*SIN(FASEDE))
      D(2,2)=CMPLX(COS(FASEDE),0.)
      M=M+1
      RETURN
      END
C
      SUBROUTINE CMAT(BETA,LS,COS,CS)
C
      COMPLEX A(2,2),YCAV
      REAL LS,BETA,COS,CS
C
      COMMON/VARS2/A
C
      BETADE=BETA*LS
      BSTUB=-(COS*1.E-3)/TAN(BETADE)
      YCAV=CMPLX(CS*1.E-3,BSTUB
      A(1,1)=CMPLX(1.,0.)
      A(1,2)=1./YCAV
      A(2,1)=CMPLX(0.,0.)
      A(2,2)=CMPLX(1.,0.)
      LS=LS/0.92
      RETURN
      END
```

```
C
C
      SUBROUTINE MATMUL(X,Y,Z)
C
C     SUBROUTINE RETURNS X=YZ
C
      COMPLEX X(2,2),Y(2,2),Z(2,2)
C
      X(1,1)=Y(1,1)*Z(1,1)+Y(1,2)*Z(2,1)
      X(1,2)=Y(1,1)*Z(1,2)+Y(1,2)*Z(2,2)
      X(2,1)=Y(2,1)*Z(1,1)+Y(2,2)*Z(2,1)
      X(2,2)=Y(2,1)*Z(1,2)+Y(2,2)*Z(2,2)
      RETURN
      END
```

APPENDIX E

COMPLETE ELEVATION PATTERNS OF 11 CAVITY ANTENNA ARRAY BY FREQUENCY AS MEASURED IN ANECHOIC CHAMBER

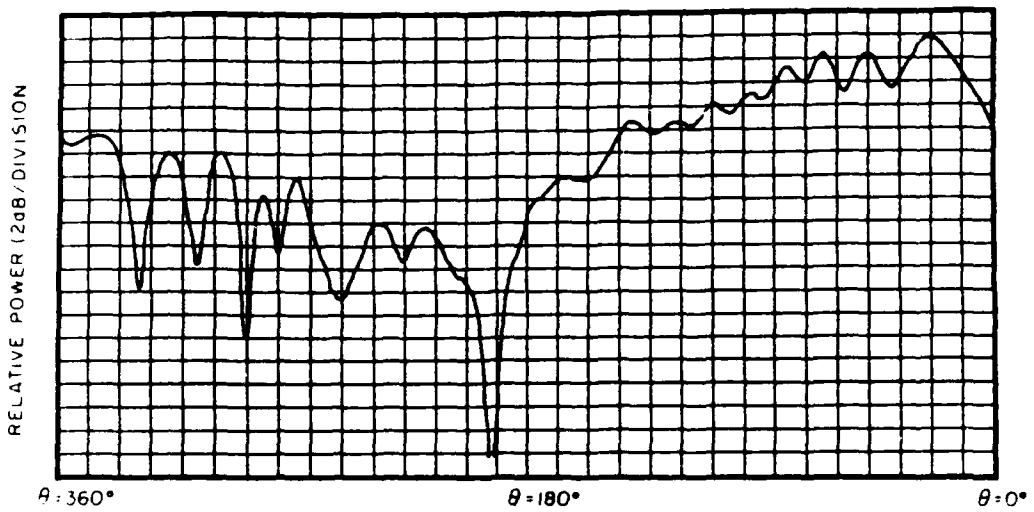

f = 1.75 GHz

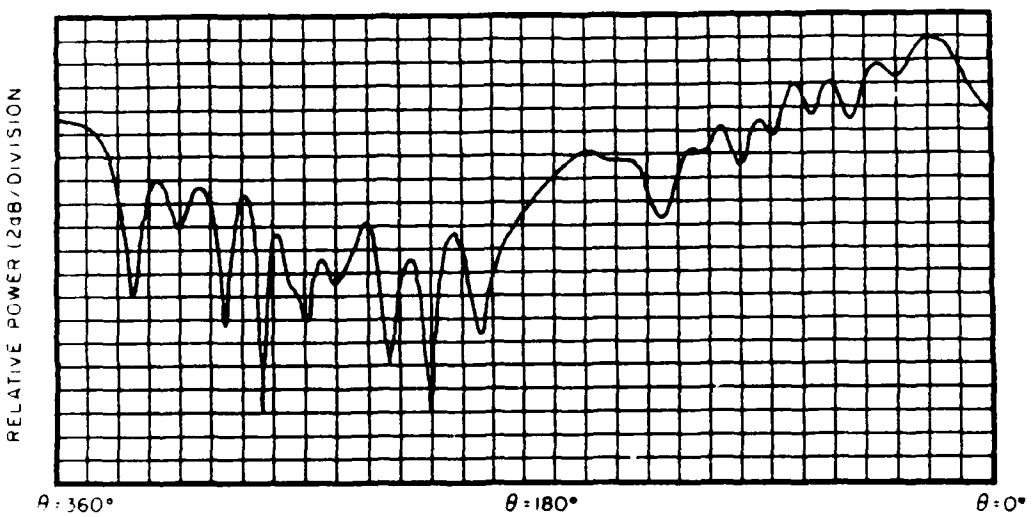

f = 2.0 GHz

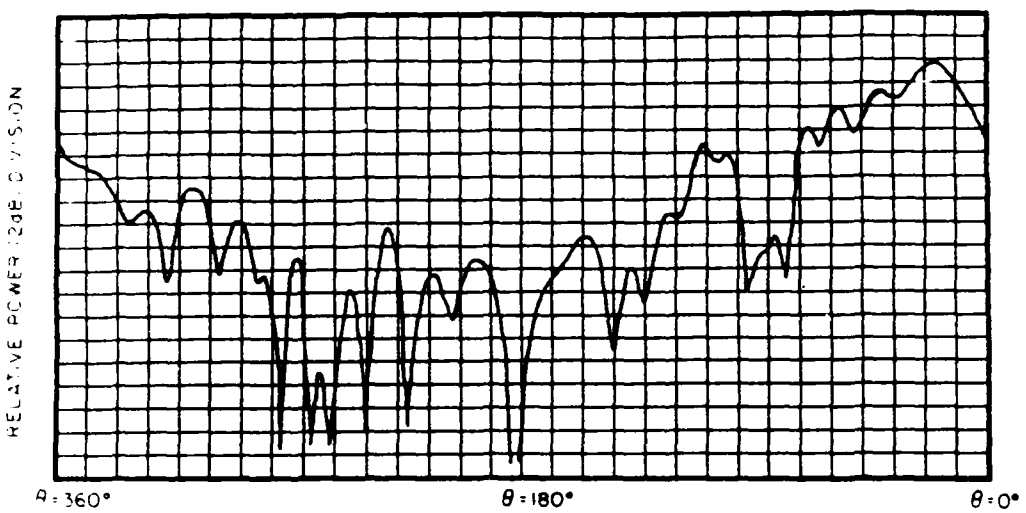

f = 2.5 GHz

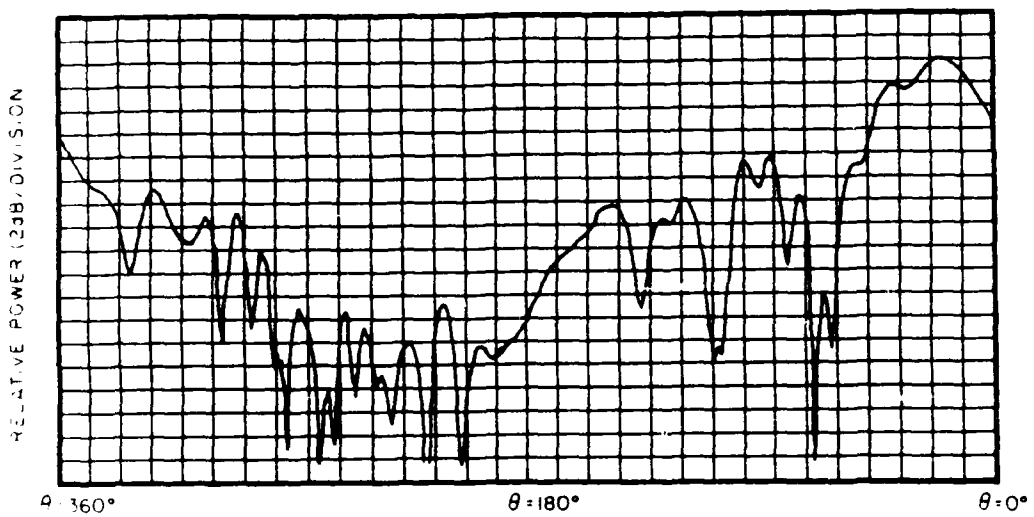

f = 2.75 GHz

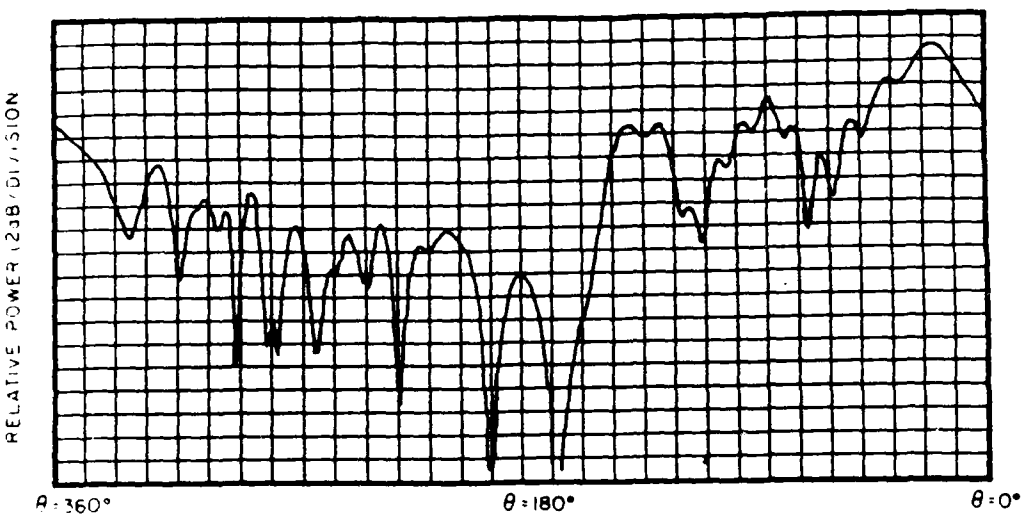

f = 3.0 GHz

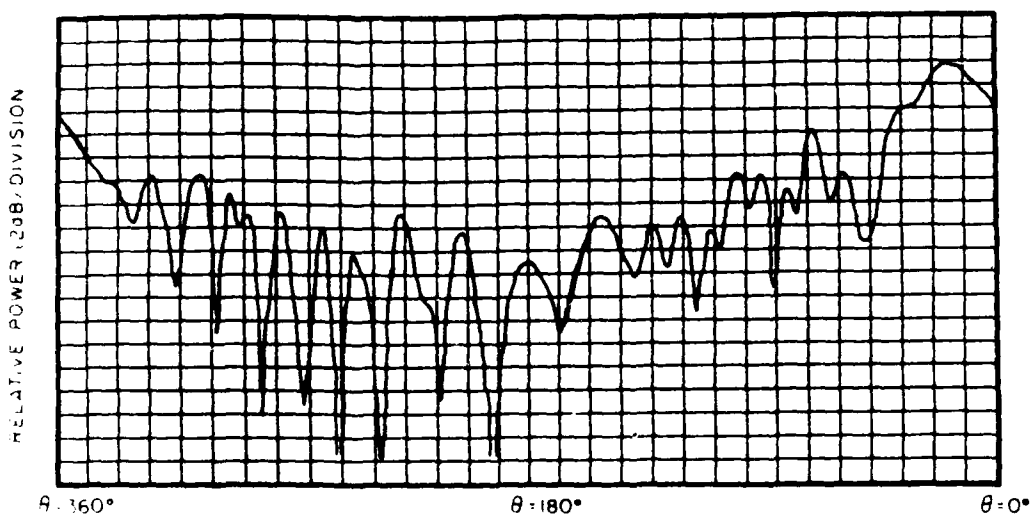

f = 3.25 GHz

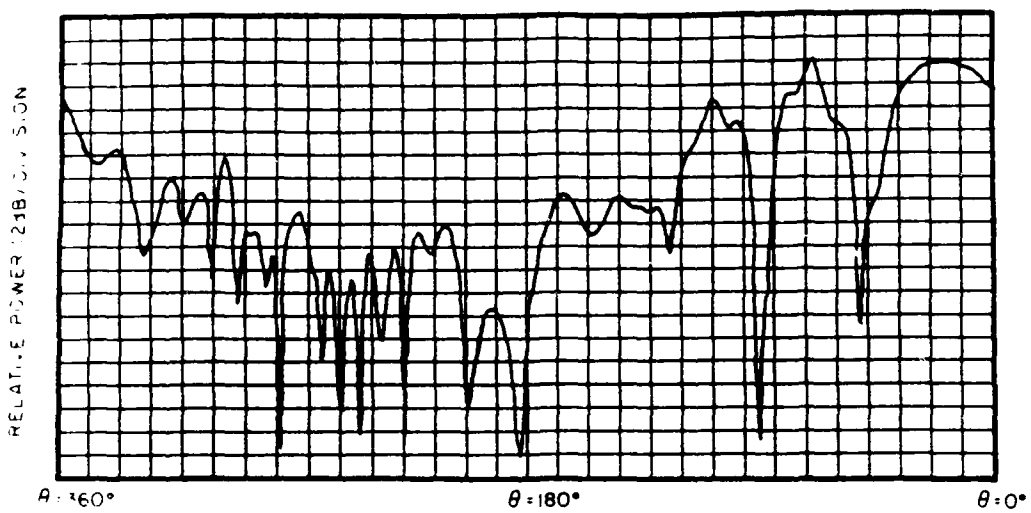

f = 3.5 GHz

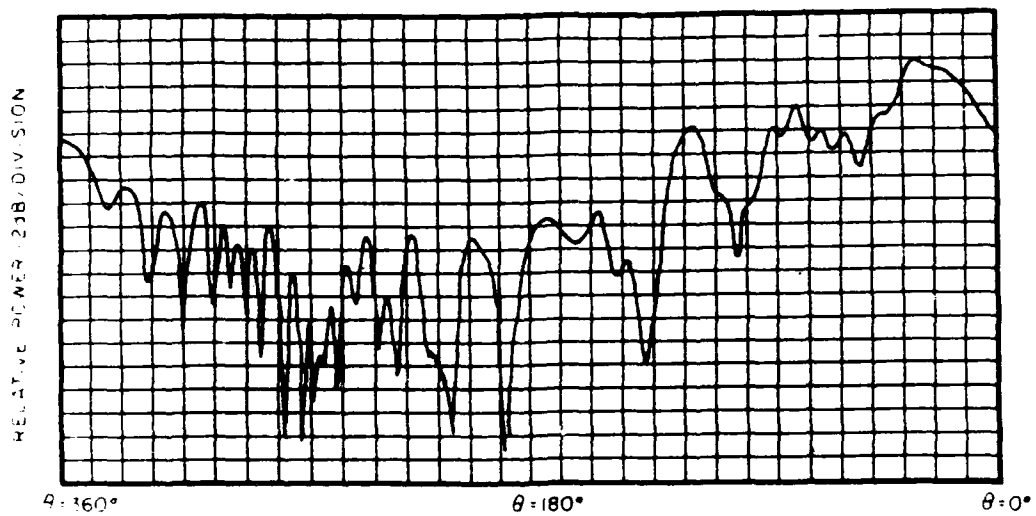

f = 3.75 GHz

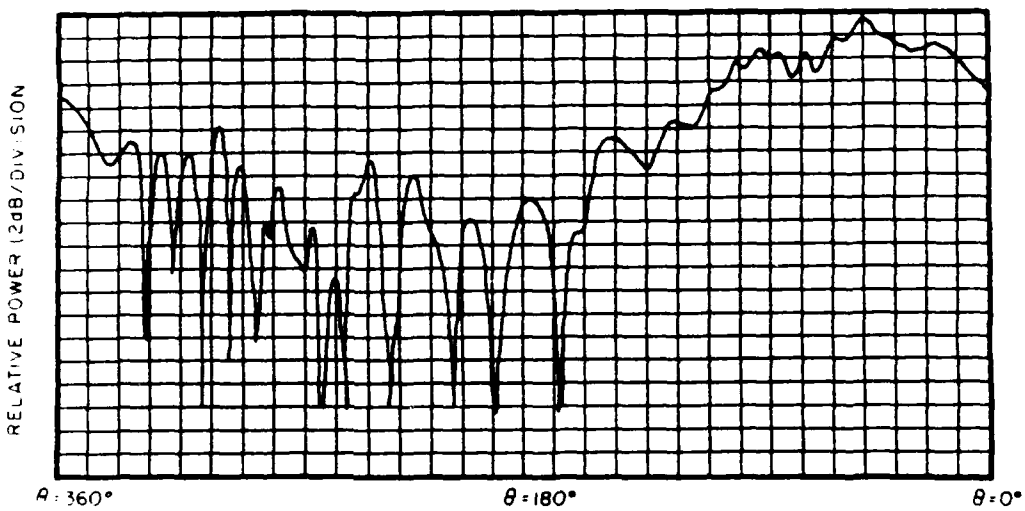

f = 3.95 GHz

REFERENCES

[1] P. E. Mayes, "Very wide band antennas for missile fuze applications," Final Report, Electromagnetics Laboratory, University of Illinois, Urbana, Illinois, Navy Contract Reqn. No. 3313-0052-00-81, Contract No. N60530-81-C-0304, 1982.

[2] P. G. Ingerson and P. E. Mayes, "Log-periodic antennas with modulated impedance feeders," IEEE Trans. Antennas Propag., vol. AP-16, no. 6, pp. 633-634, November 1968.

[3] E. Ostertag, "Experimental study of a log-periodic cavity-backed slot array with computer synthesized 50-ohm modulated impedance feeder," M.S. Thesis, Electrical Engineering Department, University of Illinois, Urbana, Illinois, 1973.

[4] D. J. Tammen, "A log periodic array of monopole-slot elements," M.S. Thesis, Department of Electrical and Computer Engineering, University of Illinois, Urbana, Illinois, 1985.

[5] T. E. Szmurlo, "A modified log-periodic cavity-backed slot antenna," M.S. Thesis, Department of Electrical and Computer Engineering, University of Illinois, Urbana, Illinois, 1986.

[6] D. Tanner, private communication.

[7] J. A. Kong, Electromagnetic Wave Theory. New York: John Wiley and Sons, Inc., 1986.

[8] W. C. Chew, "EE 350X Lecture Notes," Unpublished, Department of Electrical and Computer Engineering, University of Illinois, Urbana, Illinois, 1986.

[9] D. M. Pozar, "Microstrip antenna aperture-coupled to a microstrip line," Electron. Lett., vol. 21, no. 2, pp. 49-50, January 1985.

[10] P. L. Sullivan and D. H. Schaubert, "Analysis of an aperture coupled microstrip antenna," IEEE Trans. Antennas Propag., vol. AP-34, no. 8, pp. 977-984, August 1986.

[11] T. C. Edwards, Foundations for Microstrip Circuit Design. New York: John Wiley and Sons, Inc., 1981.

[12] P. E. Mayes, "Very Wide Band Antennas for Missile Fuze Applications," Final Report Part I, Electromagnetics Laboratory, University of Illinois, Urbana, Illinois, Navy Contract Reqn. No. 3313-0052-00-81, Contract No. N60530-81-C-0304, 1984.

[13] R. F. Harrington, Time Harmonic Electromagnetic Fields. New York: John Wiley and Sons Inc., 1965.

[14] R. J. P. Douville and D. S. James, "Experimental Study of Symmetric Microstrip Bends and Their Compensation," IEEE Trans. Microwave Theory Tech., vol. MTT-26, no. 3, pp. 175-182, March 1978.